ACS NANO

Open Access

www.acsnano.org

ARTICLE

Tunable Nanostructuring for van der Waals Materials

Gleb I. Tselikov, Anton A. Minnekhanov, Georgy A. Ermolaev, Gleb V. Tikhonowski, Ivan S. Kazantsev, Dmitry V. Dyubo, Daria A. Panova, Daniil I. Tselikov, Anton A. Popov, Arslan B. Mazitov, Sergei Smirnov, Fedor Lipilin, Umer Ahsan, Nikita D. Orekhov, Ivan Kruglov, Alexander V. Syuy, Andrei V. Kabashin, Boris N. Chichkov, Zdenek Sofer, Aleksey V. Arsenin, Kostya S. Novoselov, and Valentyn S. Volkov*

Cite This: *ACS Nano* 2025, 19, 22820–22836

Read Online

ACCESS | Metrics & More | Article Recommendations | Supporting Information

ABSTRACT: **van der Waals (vdW) materials are becoming increasingly popular in scientific and industrial applications because of their unique mixture of record electronic, optical, and mechanical properties. However, nanostructuring of vdW materials is still in its infancy and strongly depends on the specific vdW crystal. As a result, the universal self-assembled technology of vdW materials nanostructuring opens vast technological prospects. This work demonstrates an express and universal synthesis method of vdW nanoparticles with well-defined geometry using femtosecond laser ablation and fragmentation. The disarming simplicity of the technique allows us to create nanoparticles from over 50 vdW precursor materials, covering transition metal chalcogenides, MXenes, and other vdW materials. Obtained nanoparticles manifest perfectly defined crystalline structures and diverse shapes, from nanospheres to nanocubes and nanotetrahedrons. Thus, our approach illustrates a generalizable route to vdW nanostructuring with broad tunability in size, shape, and material composition, adaptable to specific application requirements.**

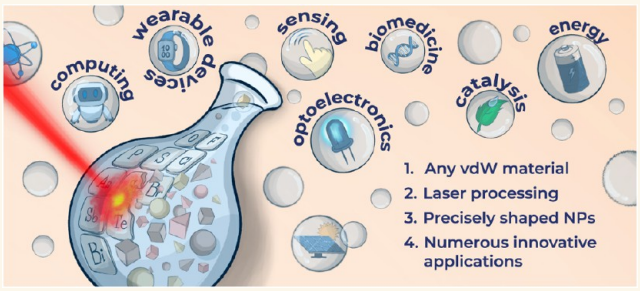

KEYWORDS: *nanoparticles, van der Waals materials, 2D materials, femtosecond laser ablation, transition metal chalcogenides, MXenes, perovskites*

The era of 2D materials exploration began with the discovery of graphene, a prominent member of the van der Waals (vdW) family of materials. vdW materials have attracted significant attention in recent years due to their extraordinary optical, electronic, magnetic, and other properties.[1−7] These materials, characterized by weak interlayer vdW forces, facilitate the creation of atomically thin layers with remarkable characteristics[8,9] that can serve as building blocks for heterostructures with on-demand properties.[10] They have been reported to exhibit giant optical anisotropy with record high in-plane and low out-of-plane refractive indices.[11−13] This feature enables them to overcome the diffraction limit, rendering them superior for various nanophotonic applications, including photonic integrated circuitry,[14,15] resonant nanoantennas,[16] light guiding,[17,18] and photodetectors.[19] Furthermore, this family encompasses a diverse range of electronic types, including record conductors such as MXenes,[20] semiconductors such as two-dimensional chalcogenides and oxides,[21] and insulators.[22] This versatility allows their use in direct ink printing to create 3D structures, which can be employed in constructing flexible and high-efficiency wireless electronics and energy storage devices.[23,24]

However, the transition from fundamental research to practical applications has been hindered by several challenges. One major obstacle is the difficulty in nanostructuring these materials, which involves the synthesis of nanostructures with the desired size, shape, and properties and is essential for their integration into advanced technologies and devices. Implementing vdW materials-based devices is further complicated by substrate interactions, which can influence their properties and performance. Additionally, controlling the thickness of these materials during synthesis is a formidable task. Chemical vapor

Received: January 9, 2025
Revised: May 22, 2025
Accepted: May 22, 2025
Published: June 16, 2025

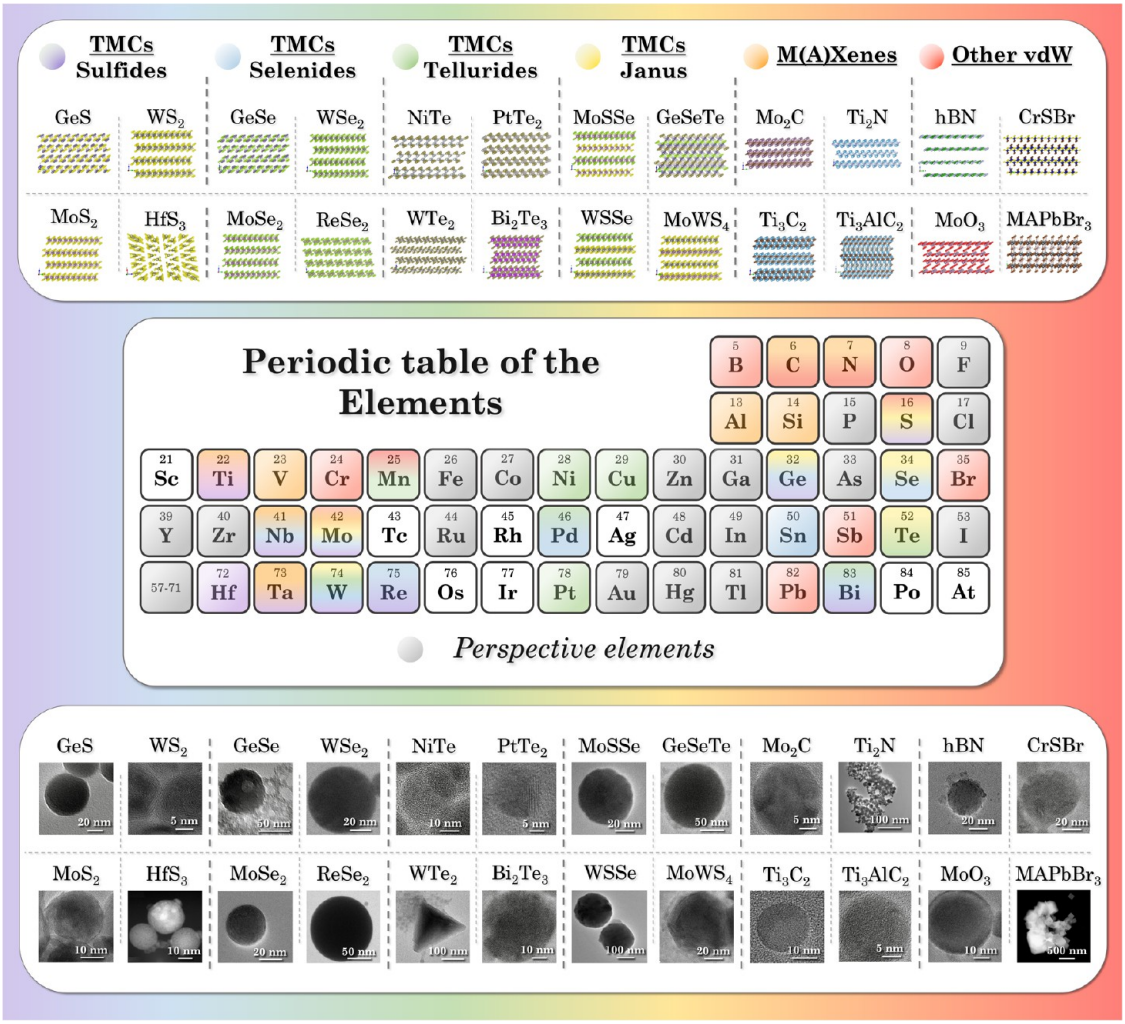

Figure 1. Schematic depiction of the periodic table (centered in a condensed format) with some prominent classes of layered materials that can be synthesized into regular NPs via laser ablation. The top part of the figure shows the crystalline structures of these materials, while the bottom part displays electron microscopy images of the NPs obtained by this method. Material classes are highlighted in color, and promising elements suitable for this technique are also marked.

deposition (CVD), a common technique for growing thin films,[25] often struggles to produce uniform and sufficiently thick vdW material films, which are crucial for specific applications. Other nanostructuring methods often necessitate bespoke protocols tailored to the unique properties of each material, requiring distinct conditions, such as temperature, pressure, and chemical environment, for the successful fabrication of nanostructures immobilized on a substrate.[26−29] Consequently, developing a universal and facile technique for nanostructuring vdW materials is highly desirable.

In this context, ultrashort pulsed laser synthesis of nanomaterials in liquids emerges as an attractive alternative to CVD methods. It stands out for its versatility and simplicity in producing nanoparticles (NPs) from a wide range of inorganic materials (metals, semiconductors, dielectrics).[30−35] The absence of toxic precursors during the synthesis process and the use of high-quality materials enable the production of ultrapure, ligand-free NPs with controlled physicochemical properties.[36,37] NPs' size, morphology, chemical composition, surface properties, and optical characteristics can be precisely tuned by adjusting synthesis parameters such as liquid media type, pulse duration, radiation wavelength and energy, and focusing conditions.[38−41] The utilization of femtosecond (fs) pulses is particularly advantageous, as it preserves the original material's crystalline structure.[30,42]

Furthermore, the pure radiation nature of laser-matter interaction and highly nonequilibrium nanocluster formation processes result in significant surface charge formed on the laser-synthesized NPs, ensuring their excellent colloidal stability.[43] Economically, the method is advantageous with advanced setups like flow cells, achieving productivity over 1 g/h for popular NPs such as gold and ceramics,[33,44] surpassing industrial wet chemistry methods, and making the technique easily scalable. Recent studies show that fs laser ablation can form spherical transition-metal dichalcogenide (TMDC) NPs, which retain the original crystalline structure and exhibit resonant optical properties.[45] Inspired by this result, we propose fs laser ablation in liquid as a versatile and effective tool to address the challenges associated with the nanostructuring of vdW materials. Its combination of simplicity, accessibility, high productivity, and the unique ability to precisely control the purity and properties of resulting nanomaterials renders this method highly valuable for a broad range of fields, including energy, catalysis, and sensing.[46−49]

https://doi.org/10.1021/acsnano.5c00546
ACS Nano 2025, 19, 22820−22836

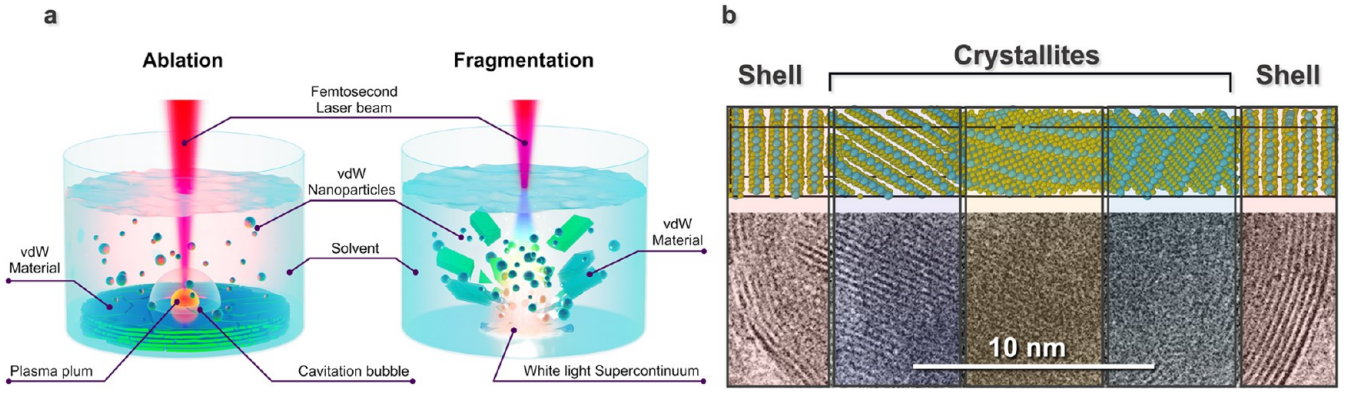

Figure 2. (a) Schematic representation of laser-driven synthesis of vdW NPs, (b) atomic structure of core−shell MoS_2 polycrystal generated in MD (top) and TEM image of MoS_2 NP (bottom).

In this work, we report the development of a universal approach that enables a fast and efficient protocol for the synthesis of NPs with the desired size, morphology, optical characteristics, and large surface-to-volume ratio, which can potentially be allied for more than 5000 members of the vdW family, overcoming the current limitations of material-specific protocols and facilitating the broader use of these materials in advanced technological applications. This approach enables the synthesis of geometrically precise NPs from a diverse set of 2D materials, including TMDCs, Janus structures, MXenes, and perovskites. Figure 1 categorizes these materials according to their structural and chemical properties, illustrating the broad applicability of our method across various classes of vdW materials. Notably, this synthesis route provides access to materials covering a substantial part of the periodic table, overcoming limitations of material-specific NP fabrication methods.

The principal classes of materials examined in this study are indicated by color coding in the upper section of Figure 1, with representative and widely studied examples provided for each category. A modified periodic table was employed to schematically illustrate the broad diversity of materials considered. Consistent with the overall color scheme, each used chemical element in the table is marked to reflect its association with one or more material classes. In cases where an element is represented by multiple colors, it signifies that this element is incorporated into compounds belonging to several distinct material classes within the scope of this work. For instance, the multicolored representation of molybdenum (Mo)—including violet, blue, yellow, orange, and red—indicates its presence in various compounds such as TMDC sulfides (MoS_2), TMDC selenides ($MoSe_2$), Janus structures (MoSSe), MXenes (Mo_2C), and other types (e.g., MoO_3).

It should also be emphasized that there is a wide range of promising materials which, although not yet experimentally explored in this work, can potentially be synthesized using our universal approach without any fundamental limitations. A variety of such promising materials are highlighted in gray on the periodic table in Figure 1. Chemical elements not marked with color were not present in the composition of commercially available vdW materials at the time of the study. Additionally, typical transmission electron microscopy (TEM) images of laser-synthesized nanoparticles from the selected material classes are shown in the lower part of Figure 1.

Here, we present over 50 samples of geometrically precise NPs derived from various vdW precursor materials, including TMDCs, MXenes, and perovskites. We experimentally confirm that the structure of vdW NPs corresponds to the initial crystals and explore their extensive potential applications. The development and integration of these NPs into devices and systems may contribute to improved performance in energy, catalysis, medicine, electronics, and environmental remediation.

EXPERIMENTAL RESULTS

Laser-Driven Synthesis of vdW NPs. The synthesis of NPs through pulsed laser ablation and fragmentation in liquids marks a significant advancement in nanomaterials engineering. The use of liquid environments in laser processing offers benefits, such as reducing heat load, confining vapor and plasma, and producing ligand-free nanomaterials with controllable properties. Recently, this method has been demonstrated to be effective for synthesizing NPs from silicon, noble metals, and other materials.[40,50−52] Here, we elucidate the processes of laser ablation and fragmentation, their mechanisms, and the inherent advantages of using ultrashort fs laser pulses.

The laser ablation process involves exposing a bulk target to focused fs laser radiation, which scans the surface of the crystalline target immersed in liquid (Figure 2a). This interaction causes material to eject from the target into the liquid, undergoing various transformations before eventually forming colloidal NPs.[26,38] Using fs pulses is particularly advantageous in this method, as it minimizes thermal effects, thereby preserving the structural integrity of the ablated material.[30,42] For instance, a recent study has demonstrated that fs laser ablation can produce spherical TMDC NPs, which retain the original crystal structure and display resonant optical properties.[45]

When the fs laser pulse ($>10^9$ W/cm^2) interacts with the target surface, it generates plasma originating from the initial material with extremely high local temperature and pressure. As the plasma decays, it transfers energy to the liquid, forming a cavitation bubble.[53] The vapor inside the bubble encloses a region in which solid crystallization and formation of atom clusters occur (Figure 2a). The combination of high pressure, temperature, and plasma density, followed by rapid cooling, creates an ideal thermodynamic environment for the formation of metastable phase nanomaterials (e.g., hexagonal close-packed Ni, Au−Si alloy),[54,55] which are challenging to achieve through conventional chemical methods. During laser ablation in liquids, a small fraction of the ablated material undergoes chemical oxidation at the NPs' surface, even for noble metals.[42] These minor surface modifications generate an intrinsic surface charge that fosters electrostatic repulsion and stabilizes the colloidal dispersion, rather than promoting agglomeration. Nonetheless, most of the colloidal material retains the chemical composition of the initial targets, including multicomponent vdW materials.

https://doi.org/10.1021/acsnano.5c00546
ACS Nano 2025, 19, 22820−22836

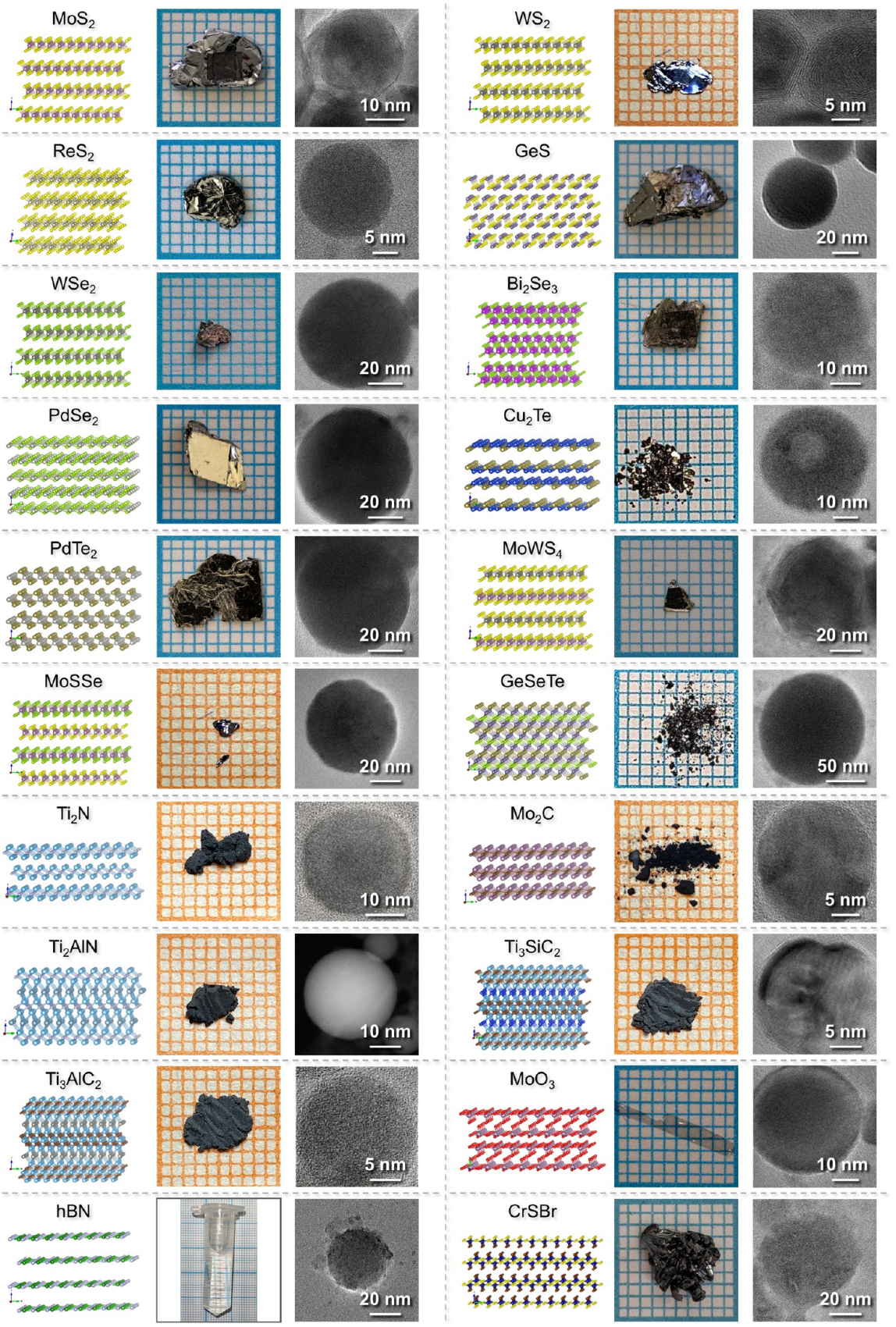

Figure 3. Three-dimensional representation of the crystal structure of vdW materials, pictures of initial crystals/powders/solutions, and TEM image of laser-synthesized vdW NPs.

https://doi.org/10.1021/acsnano.5c00546
ACS Nano 2025, 19, 22820−22836

Alternatively, laser fragmentation involves directing laser pulses into a liquid containing a homogeneously distributed vdW material in powder form.[56] In this process, NP formation is triggered by microparticles within the liquid absorbing the laser energy. Fs pulses induce nonlinear phenomena in the liquid, including self-focusing, filamentation, and the generation of a white light supercontinuum, which enhances energy absorption and promotes NP formation. This broad wavelength range allows the initial radiation energy to be effectively absorbed by nearly any source material (Figure 2a). The primary mechanisms of NP formation in this process are Coulomb explosion and photothermal evaporation. According to the liquid-drop model for the Coulomb explosion, a multiply charged particle ejected from the initial educt becomes unstable when the disruptive Coulombic force of charge repulsion exceeds the attractive cohesive force. While this mechanism is dominant at high laser intensities typical for the fs regime and relatively small particle size (<50 nm), the photothermal evaporation is mainly related to the ns pulse duration and large educt particles. Therefore, this approach offers a unique opportunity to fabricate NPs in mobile colloidal form with controlled size, uncontaminated surface, and high stability.

Laser fragmentation can serve as an additional step to refine the size characteristics of preformed nanomaterials. By extending the fragmentation duration, both the mean size and the width of the size distribution can be controlled across a broad range.[38,41] Additionally, employing longer pulse durations in the nanosecond regime enables laser-induced melting in liquids, facilitating the synthesis of alloy NPs with distinctive composite properties.[57] In the case of laser ablation in liquids, increasing the pulse energy results in a broader size distribution of NPs and the emergence of a distinct bimodal profile.[41] This effect may be attributed to the expansion and prolonged lifespan of the cavitation bubble, which influences the formation of larger NPs and promotes surface fragment detachment from the target due to photomechanical effects.[58] On the other hand, the most precise control over NP size can be achieved via laser-induced forward transfer (LIFT) into liquids. Conventional LIFT enables the precise deposition of single NPs with well-defined sizes onto a substrate. A novel approach, recently introduced by B. Chichkov,[59] extends this concept by enabling the direct deposition of monodisperse NPs into liquid media during the laser ablation of thin foils, opening new possibilities for the fabrication of colloidal NPs with highly controlled size distributions.

We synthesized stable colloidal solutions of NPs from vdW materials using pulsed laser ablation and fragmentation in liquids (Methods), applied to solid targets, powders, and solutions (Figure 2a). The characteristics of the NPs—such as size, shape, and specific properties—can be finely tuned by adjusting various parameters. These include the nature of the target material, laser power, exposure duration, and the liquid medium's composition. By tailoring these parameters, NPs can be customized to meet the specific requirements of applications ranging from electronics to pharmaceuticals.

To study the mechanism of MoS_2 NPs crystallization in detail and to characterize the influence of the cooling regime on its structure, we utilized classical molecular dynamics (MD) with the state-of-the-art machine-learning interatomic moment tensor potentials (MTPs).[60,61] This method enables large-scale MD simulations over tens of nanoseconds with accuracy approaching that of density functional theory (DFT). Further details on the calculation parameters are provided in the Methods section.

We performed a series of MD simulations, cooling the MoS_2 melt from $T = 2300$ K (slightly above the melting point) down to complete crystallization (Figure S3). The cooling rate was varied in the range of 0.08−2 K/ps (see the video of the MD simulation in the Supporting Information (SI)). Our results indicate that crystallization can be divided into two competing processes: the formation of ordered MoS_2 layers on the droplet surface, aligned parallel to the phase boundary (heterogeneous nucleation—"shell" in Figure 2b), and the formation of randomly oriented crystallites within the bulk (homogeneous nucleation—"crystallites" in Figure 2b). The interplay of these processes leads to a core−shell structure, where the core-to-shell ratio and the average size of crystallites in the core depend on the cooling rate (Figure S4). Lower cooling rates result in a thicker shell and larger inner crystallites, whereas higher rates produce a thinner shell and smaller inner crystallites. This demonstrates that the cooling process can modulate the nanostructure parameters of NPs and their optical properties. The heterogeneous nature of shell nucleation results from the presence of the solvent-NP boundary, whereas inner crystallites form homogeneously within the bulk.

Versatility of the Laser Ablation Method for the Synthesis of vdW NPs. Despite the extensive quantitative and structural diversity of vdW materials, laser synthesis in liquid facilitates the production of stable colloidal NPs from a wide range of materials. The laser-matter interaction mechanism, which involves material removal from the target surface, highlights the versatility of this approach. Moreover, the flexibility of laser synthesis in liquid enables processing of metals, semiconductors, and dielectrics in different forms, such as bulk crystalline targets, powders, and liquid suspensions.

In this study, we present the synthesis of geometrically precise NPs from over 50 materials. These materials include TMDCs (sulfides, selenides, tellurides, and Janus structures), M(A)Xenes, and other promising compounds such as hBN, MoO_3, $MAPbBr_3$, and CrSBr. Figure 3 depicts the most prominent vdW materials along with their crystal structures, photos of the initial materials, and TEM images of the resulting NPs, thereby confirming the versatility of the laser synthesis method. A comprehensive overview of all synthesized materials, categorized by class, is provided in Figure S1.

In addition to the fundamental ability to synthesize colloidal solutions of vdW NPs, we demonstrate the capacity to control the size and optical properties of the resulting nanomaterials. By varying the liquid medium, we can tune the size distribution, compositional properties, and optical extinction spectra of the NPs. For instance, employing laser ablation of MoS_2 in different solvents yields NPs of various sizes: (75 ± 41 nm) in water, (42 ± 24 nm) in acetone, and (15 ± 9 nm) in acetonitrile (Figure S2a).

The dependence of NPs size characteristics on the solvent type is a well-documented phenomenon in laser synthesis in liquids.[38,62] Typically, the reduction in NP size in organic solvents is attributed to the early capping effect, where solvent molecules or their products of local decomposition interact with the NP surface immediately after laser-target interaction, inhibiting further growth.[63] In this context, these products act similarly to surfactants, which are commonly used to regulate the growth process and control the size characteristics of laser-synthesized nanomaterials.[39] However, the zeta potential of NPs generally does not exhibit a strong dependence on the solvent type and tends to retain the same charge sign for a given material.[38] Variations in absolute zeta potential values are primarily linked to differences in lattice defect formation and surface modifications that occur during NP synthesis in different liquid media.

Furthermore, altering the liquid medium type during synthesis allows modulation of the optical and compositional properties of the NPs. Laser fragmentation of WS_2 in acetonitrile produces ultrasmall quantum dots exhibiting a distinct excitonic resonance in the near-infrared (NIR) region, peaking at around 670 nm (Figure S2b). The choice of solvent significantly affects the size distribution of NPs, which in turn leads to a dramatic change in extinction characteristics, as illustrated in Figure S2a,b. Simultaneously, use of liquid media with higher oxygen content, both in the composition and dissolved state, leads to the formation of an oxide layer on the surface of nanoparticles, even in the case of noble metals.[42] This surface modification process can be largely controlled by selecting different liquid media type, as demonstrated with alternative plasmonic and van der Waals materials.[50,64] The dependence of oxygen content from the solvent used during the laser synthesis of Ti_3C_2 MXene nanoparticles is illustrated in Supplementary Figure S2c. Additionally, certain organic solvents, such as hexane or toluene, may cause carbonization of the nanoparticle surface during laser synthesis.[65] This method provides further control over the optical properties of nanoparticles in relation to their size characteristics. Specifically, synthesis in acetone produces WS_2 NPs with a peak in extinction signal near 750 nm, whereas water-based fabrication results in an extinction spectrum resembling Rayleigh scattering. Notably, laser synthesis offers the

https://doi.org/10.1021/acsnano.5c00546
ACS Nano 2025, 19, 22820−22836

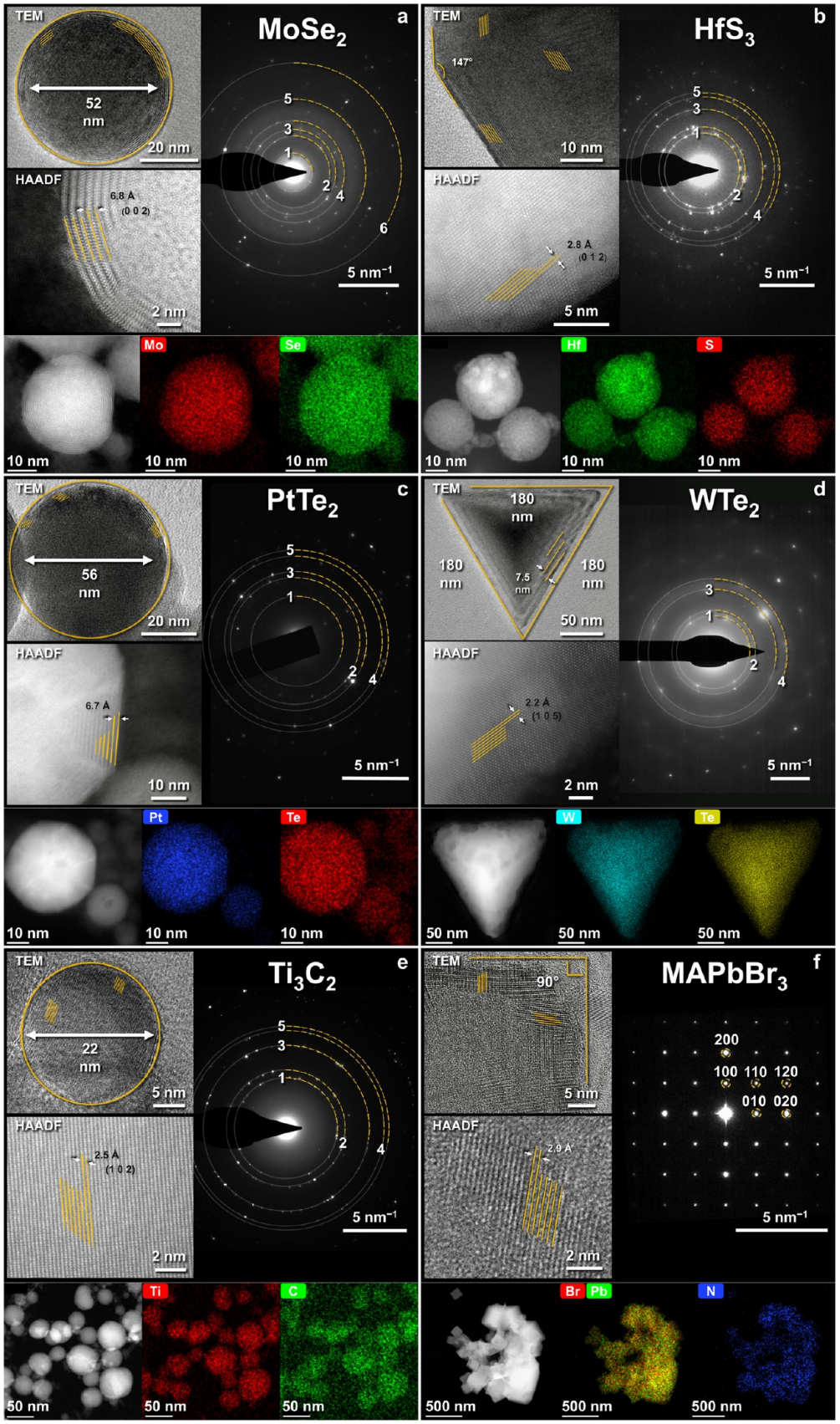

Figure 4. Structural and compositional analysis of laser-synthesized vdW NPs. Each panel includes TEM, HAADF, SAED characterizations, and EDX analysis.

https://doi.org/10.1021/acsnano.5c00546
ACS Nano 2025, 19, 22820−22836

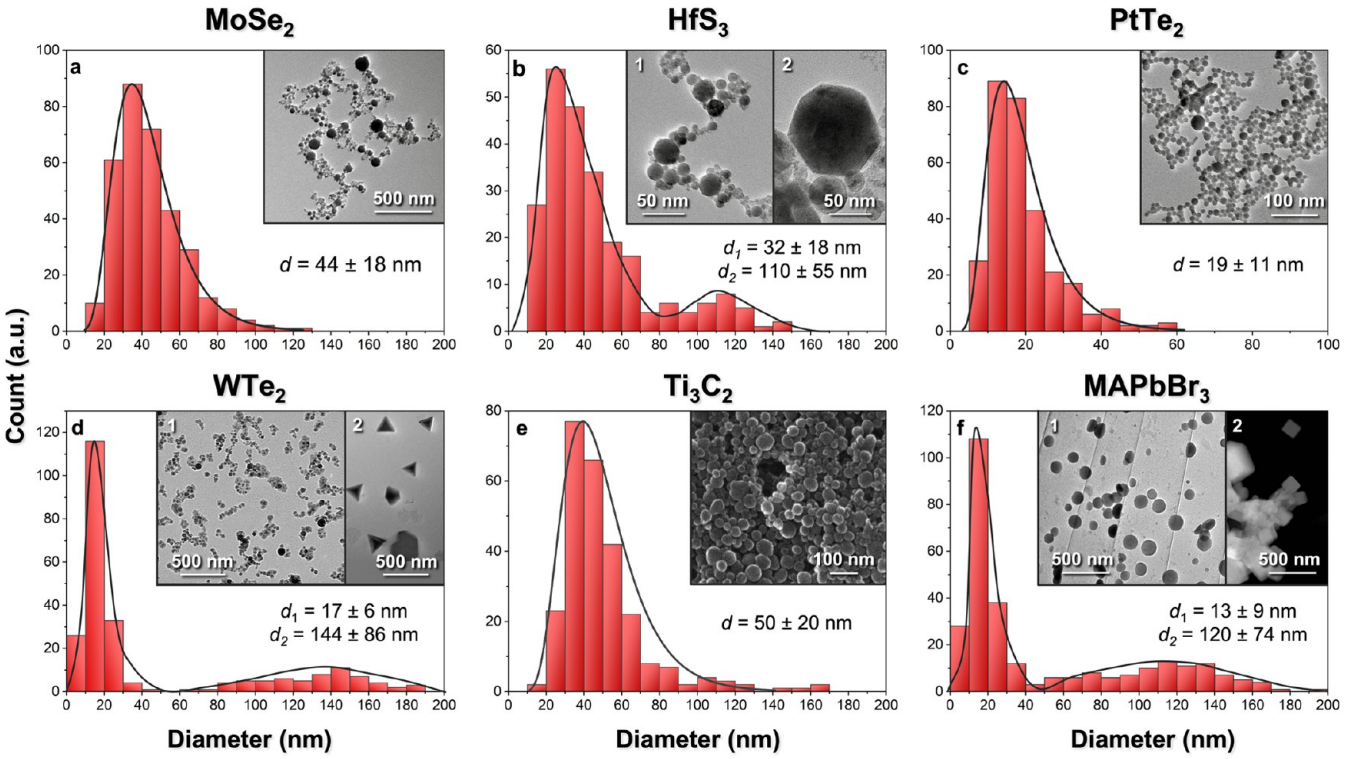

Figure 5. Size distribution and representative TEM/SEM image of laser-synthesized vdW NPs.

advantage of producing stable NPs with uncompensated surface charges, which was validated across various obtained vdW NPs through Zeta-potential measurements (Figure S2d). This research expands the utility of laser synthesis in advancing nanomaterial development, offering a spectrum of properties and potential applications across diverse fields.

Morphology and Structure of vdW NPs. During the experiments, we observed that within seconds of operating the high-repetition-rate laser, the liquid medium rapidly changed color, indicating the formation of NPs. The colloidal solution color varied by material and liquid medium, from greenish-brown for $MoSe_2$ in acetone to sky-blue for Ti_3C_2 in water. These distinct colors suggest that the NPs retain the optical characteristics of their source materials. We recently demonstrated that a simple centrifugation step can effectively isolate different size fractions of MoS_2 NPs.[45] At the same time, variation in the duration of the MoS_2 powder fragmentation opens avenues for extra control of the dimensional, optical, and compositional characteristics of the resulting NPs.[64] These modalities unlock the ability to produce 5−10 nm quantum dots with pronounced exciton resonances in the NIR region and spherical NPs exhibiting Mie resonances in the visible and NIR regions.[45,64]

To thoroughly investigate the morphology and structure of the laser-synthesized vdW NPs, we utilized high-resolution transmission electron microscopy (TEM), high-angle annular dark-field imaging (HAADF), selected area electron diffraction (SAED), and energy-dispersive X-ray spectroscopy (EDX) analysis (Methods). The results indicate that NPs synthesized from various vdW materials—including TMDCs, M(A)Xenes, perovskites, transition metal oxides, and Janus structures—exhibit high crystallinity, retaining crystallographic planes and chemical compositions corresponding to the initial materials (Figure 4; Table S1).

Notably, nanostructures from different materials displayed diverse morphologies, ranging from spherical and fullerene-like shapes to nanotetrahedrons, cubes, and polygons (Figure 4). For instance, laser-ablated $MoSe_2$ (Figure 4a) and $PtTe_2$ (Figure 4c) NPs exhibited fullerene-like polygonal structures that were nearly spherical. TEM images revealed the layered crystalline structure of these nanostructures. EDX analysis and SAED patterns confirmed the chemical composition consistency, while HAADF imaging revealed atomic-resolution contrast, allowing individual atoms to be distinguished in the shell of a $MoSe_2$ nanoparticle and to identify the interlayer distance of 6.8 Å. Conversely, laser fragmentation of Ti_3C_2 powder resulted in the formation of purely spherical single-crystalline NPs which are clearly visible on the HAADF image (Figure 4e). EDX analysis verified that the atomic composition matched the original material. Additionally, SAED analysis confirmed the high crystallinity of the NPs and the correspondence of the diffraction rings to the pure Ti_3C_2 diffraction pattern (Table S1).

A different situation was observed for HfS_3, WTe_2, and perovskite $MAPbBr_3$ (Figure 4b,d,f). In the case of HfS_3, we obtained polygonal nanostructures with 6−12 facets. A significant quantity of spherical NPs, which is the most typical morphology for laser synthesis in liquid, was also present. These NPs exhibited a pronounced crystalline layered shell as revealed by HAADF analysis. SAED characterization confirmed the high crystallinity of the resulting NPs and the similarity of diffraction patterns to the initial material. EDX images revealed the material composition, consisting of Hf and S.

In contrast, laser ablation of a solid WTe_2 crystal resulted in the formation of equilateral nanopyramids with average side lengths of 180 nm (Figure 4d). These nanopyramids exhibited a stepped structure with an average pitch of 7.5 nm, as evident in the TEM image. HAADF analysis revealed the perfect crystallinity of the nanopyramids, while EDX and SAED confirmed the intact chemical composition. Another noteworthy result was the formation of cubic NPs based on perovskite $MAPbBr_3$. These nanostructures also had a pronounced crystalline structure, clearly visible in TEM and HAADF images. EDX analysis confirmed the consistency of the original composition, showing the presence of Pb, Br, and N. A detailed analysis of the SAED pattern is presented in Supplementary Table S1.

We attribute the observed differences in the shell shape of the nanoparticles to the mechanical properties of the monolayer materials—specifically, their bending modulus and resistance to out-of-plane deformation. We hypothesize that materials with a higher bending modulus tend to preserve a spherical shell shape, whereas more easily bendable materials are prone to forming polygonal geometries (see Supplementary Note 1 for details).

https://doi.org/10.1021/acsnano.5c00546
ACS Nano 2025, 19, 22820−22836

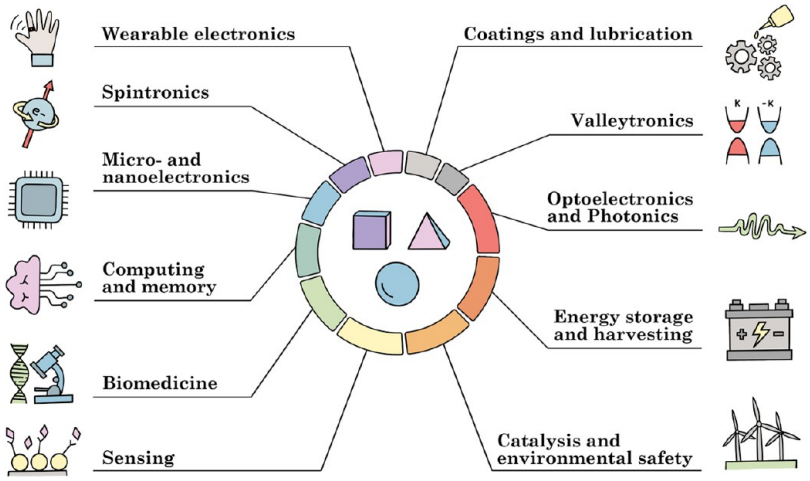

Figure 6. Potential applications of geometrically precise vdW NPs. The pie chart categorizes the application sectors based on an analysis of over 3000 scholarly articles related to TMDC nanoflakes or nanomaterials. The relative sizes of the pie chart segments qualitatively represent the frequency of each application mentioned in the literature. The "Other" category is not displayed in this diagram.

Despite the variety of morphologies observed above, spherical NPs remain the most dominant and typical shape of nanomaterials produced by laser synthesis (Figure 3). Moreover, different morphological fractions of laser-synthesized NPs can be easily isolated by centrifugation due to their various size characteristics. For instance, spherical NPs typically exhibit relatively small sizes, controllable within the 2−100 nm range. SEM and TEM analyses revealed that the obtained vdW nanostructures exhibit a log-normal size distribution, with modes generally less than 50 nm and relatively narrow size distributions within the spherical fraction (Figure 5). Specific size distribution characteristics (mode ± fwhm) include (44 ± 18) nm for $MoSe_2$ (Figure 5a), (19 ± 11) nm for $PtTe_2$ (Figure 5c), (50 ± 20) nm for Ti_3C_2 (Figure 5e). NPs based on HfS_3, WTe_2, and $MAPbBr_3$ demonstrated a bimodal size distribution with values of (32 ± 18) nm and (110 ± 55) nm (Figure 5b), (17 ± 6) nm and (144 ± 86) nm (Figure 5d), (13 ± 9) nm and (120 ± 74) nm (Figure 5f), respectively. The second peak is associated with the presence of polygonal nanostructures of HfS_3 (Figure 5b, inset 2), nanopyramids of WTe_2 (Figure 5d, inset 2), and nanocubes of $MAPbBr_3$ (Figure 5f, inset 2), reflecting a different morphological mode typical for a particular material. Notably, no signs of precipitation were observed for several months after synthesis when these colloidal nanostructures were stored in a refrigerator, indicating the stability of all reported size fractions.

Furthermore, we highlight that laser ablation and fragmentation in liquids are highly adaptable techniques that can be easily scaled up. The efficiency of laser synthesis is strongly influenced by the material type, porosity, and laser parameters, including energy, fluence, wavelength, pulse duration, and focusing conditions.[38,66] For instance, the setup described in this work achieves production rates of 40 mg/h for MoS_2, 35 mg/h for WSe_2, and up to 100 mg/h for Au. In laser fragmentation, typical production rates are 20 mg/h for Ti_3C_2 and 25 mg/h for Ti_3AlN_2.

Moreover, integrating a flow cell geometry with high-energy, high-repetition-rate laser pulses significantly enhances productivity, reaching several grams per hour for commonly processed materials such as copper and ceramics.[33,44] This approach can also be applied to vdW materials, with an expected increase in yield. Notably, when production rates exceed 550 mg/h, laser-assisted synthesis becomes more cost-effective than industrial wet chemistry methods for gold NPs.[66] Furthermore, for synthesizing spherical, colloidally stable NPs from vdW materials, laser synthesis remains the only known viable method. Thus, this technique enables the practical use of NPs in applications requiring precise shape and controlled dimensions.

Thus, we have demonstrated that a relatively simple method, specifically laser ablation or fragmentation, can be effectively used to synthesize NPs from a wide range of vdW materials. A distinguishing feature of these NPs is their well-defined geometric shapes, controllable sizes, and resistance to aggregation. Combined with the inherent properties of vdW materials, these characteristics enable their use in a broad range of applications. In the following section, we will briefly explore some of the most promising areas for their use.

DISCUSSION

The ability to fabricate NPs with well-defined shapes from vdW bulk materials broadens their applicability across various technological fields, owing to properties such as semiconductor behavior, high surface area, and tunable band gaps. By manipulating the size, shape, and composition of these NPs, their properties can be finely tuned to meet specific needs, making them desirable for advanced applications. These NPs are already compatible with various technologies that utilize precisely shaped NPs.[45,67] Figure 6 illustrates some of the most promising sectors for the application of vdW NPs, including diverse electronics, environmental technologies, novel computing, sensors, biomedicine, and more. Below, we will briefly explore some of these NPs' most intriguing application possibilities.

Catalysis. Photocatalysis is a prominent method for addressing water pollution through natural sunlight.[68] vdW NPs exhibit exceptional catalytic properties due to their high surface area and active sites.[45] By adjusting the shape and composition of these NPs, their catalytic activity and selectivity for specific reactions can be optimized, potentially leading to more efficient and sustainable industrial processes. Moreover, vdW materials are gaining recognition for their ability to generate hydrogen via photocatalytic water splitting, presenting a more economically viable alternative to traditional photocatalysts.[69,70] For example, MoS_2 and $MoSe_2$ are notable for their widespread availability, affordability, robust physicochemical stability, and low bandgap energy (1.6 eV), making them prime candidates for such applications.[71,72]

Additionally, vdW materials hold promise for water electrolysis. For instance, due to a lower onset potential, a combination of MoS_2 NPs with graphene-like substances[73] enhances the hydrogen evolution reaction (HER) activity beyond that of standalone MoS_2. The smaller size of TMDC NPs contributes to their extensive surface area, reducing the distance for charge transfer and thereby accelerating the water-

https://doi.org/10.1021/acsnano.5c00546
ACS Nano 2025, 19, 22820−22836

splitting process. A large specific surface area favors the adsorption of organic pollutants and facilitates electron transport.[74] Consequently, developing an economical method for producing such NPs is crucial for both scientific and practical reasons. Laser ablation has emerged as a highly effective technique in this context, underscoring its significant application value.

Sensing. In environmental monitoring, food quality assurance, healthcare, pharmaceutical analysis, and other fields, the role of chemical sensors and biosensors is increasingly critical.[75] Semiconductor-based sensors are appealing due to their cost-effectiveness and simple operational principles, which rely on variations in conductance upon exposure to specific gases.[76] vdW NPs are particularly noted for their applicability across a spectrum of sensing technologies.[77] Numerous vdW-derived NPs have been engineered to refine electrochemical biosensors, given their minimal noise interference and enhanced carrier mobility.[78] Furthermore, vdW materials are excellent for creating energy-efficient, flexible gas sensors that operate at room temperature, a particularly challenging capability with metal oxides.

Studies on 2D TMDCs such as MoS_2, $MoSe_2$, WS_2, and WSe_2 have shown that these materials surpass others in sensitivity, selectivity, and response speed, making them ideal for flexible and wearable gas sensors.[79] When NPs are combined with materials like graphene, gas detection sensitivity can be further enhanced. Additionally, vdW NPs can be used for electrochemical biosensors for DNA analysis when incorporated into composites with graphene or CNTs.[80] Photoelectrochemical sensing, which operates under visible light, requires photocatalysts such as vdW NPs. Notable innovations include WS_2-graphene nanosheets and gold NPs for the label-free electrochemical determination of IgE.[81] Moreover, $MoSe_2$-graphene composites have shown efficacy in sensing PDGF-BB.[82] Consequently, vdW NPs exhibit significant potential for advancing a broad array of sensing applications, underscoring their critical role in the future development of sensor technology.

Energy. In the energy sector, vdW NPs play a crucial role in enhancing the performance of energy storage and conversion devices, such as lithium-ion batteries (LIBs), supercapacitors, and solar cells. The large surface area of the NPs improves interaction with electrolytes, boosting both the storage capacity and rate capability. Additionally, the tunable band gaps of TMDCs allow for the fine-tuning of solar cells' absorption spectra, potentially elevating their efficiency.[83] For instance, materials such as MoS_2 and WS_2 possess these properties and a high density of reactive sites at their edges, making them ideal for electrochemical reactions. The interlayer spacing in TMDCs accommodates lithium ions without significant volume expansion, outperforming silicon-based alloys. Studies have shown[84] that MoS_2, combined with carbon, has enhanced performance, underscoring its reliability as a material for flexible LIBs.[85] The exceptional surface-to-volume ratio and uniform shape of vdW NPs are expected to improve LIB performance further, providing superior control and reproducibility.

For supercapacitors, where the electrode's composition is critical to the system's overall performance,[86] vdW materials are also highly effective. Although carbon-based materials are commonly used as electrodes, they suffer from low energy density. TMDCs, including WS_2 and MoS_2, provide numerous active sites for charge storage and channels for ion exchange, leading to significantly high specific capacitance due to rapid redox reactions. The electrode material's high surface area and porosity enhance ion transport, thereby increasing capacitance.[87] The electrochemical properties of geometrically precise vdW NPs, especially when combined with carbon materials, are considered superior, although extensive research is needed to validate this.

Computing. vdW NPs, with their adjustable band gaps, are pivotal in advancing next-generation electronics and optoelectronic devices. This is especially true in the emerging field of bioinspired neuromorphic computing systems (NCSs) and resistive random-access memory (RRAM) devices.[88] vdW materials bridge the gap between conventional and neuromorphic electronics as foundational components for memristors, thin-film transistors, photodetectors, and other essential devices. NCSs mimic human neural architectures through computing-in-memory.[88] Memristors, in turn, emulate synapses via resistive switching (RS) effects, promoting a shift from von Neumann's paradigm.[89] This transition supports the development of devices for diverse applications in robotics, the Internet of Things (IoT), biomedicine, and more.[90] The high electronic mobility, exceptional light absorption, and tunable conductance of vdW materials make them ideal for RS technology, enabling ultralow power consumption.

Numerous vdW materials have been proposed as the basis for memristors.[91] Notable examples include $MoSe_2/MoS_2$ heterostructures;[91] $MoSe_2$ nanoislands,[92] nanorods,[93] nanosheets,[94] and nanocomposites;[95] $MoSe_2$/PVA systems[96] with varying NPs[97] concentrations; and guar gum-WTe_2 nanoflakes hybrids.[98] Structures based on vdW materials can also be utilized as photonic electrical switches.[99] For instance, an NIR photonic RRAM device incorporating MoS_2 with $NaYF_4$:Yb^{3+}, Er^{3+} upconversion NPs, demonstrated stable NIR light-controlled RS.[100] Additionally, Bi_2S_3 and Bi_2Se_3 NPs, known for their strong NIR absorption, also indicate potential applications in NIR RRAM.[101,102] Utilizing NPs increased the maximum I_{on}/I_{off} ratio[96] and decreased the operating voltages[98] of memristors, thus indicating the superiority of NPs in this area. Using NPs of the correct shape may enhance RS's stability and reproducibility, addressing a significant challenge in contemporary memristor devices. In conclusion, vdW NPs can significantly advance NCSs and RRAM devices, enhancing performance and efficiency in next-generation electronics and optoelectronics.

Nanocomposites. Like other NPs, vdW materials possess a broad potential for use as nanocomposites, a potential that is yet to be fully explored due to the vast number of possible combinations. For instance, in photocatalysis, heterojunction composites benefit from the disparate energy levels of two semiconductors merging to create a system that promotes swift and effective charge separation, reducing the recombination rate of electron−hole pairs.[71] This leads to a notable enhancement of photocatalytic activity. Similar charge separation strategies have been applied to traditional oxide composites like TiO_2/MoO_3.[103] Various TMDC composites have been evaluated for their photocatalytic efficiency under visible light, such as MoS_2/BiOBr,[104] MoS_2/rGO,[105] and MoS_2/C_3N_4.[106] Nanocomposites, where NPs are embedded into a matrix, such as a polymer, have also demonstrated their potential in the development of energy-efficient memristors, as seen in the $MoSe_2$/PVA composite.[96] Huge opportunities also arise from combining TMDCs, MXenes, and perovskites, especially with polymers, for various biomedical applications,

https://doi.org/10.1021/acsnano.5c00546
ACS Nano 2025, 19, 22820−22836

sensing, industrial uses, and more. Controlling the shape and size of the particles will enable the achievement of stable and reproducible results.

Biomedicine. The tunable optical and chemical properties of vdW-based nanostructures extend their biomedical applications beyond sensing to include advanced therapies such as drug delivery, photothermal therapy (PTT), photodynamic therapy (PDT), and radiation therapy (RT), as well as diagnostics like computed tomography (CT), magnetic resonance imaging (MRI), and photoacoustic imaging (PAI).[107,108] Unlike traditional plasmonic metals, vdW nanomaterials absorb dominantly in the NIR range, enhancing PTT and PAI for noninvasive theranostics of deep-seated tumors.[107−110] For instance, we recently demonstrated that MoS_2 NPs have shown nearly double the photothermal response compared to Si NPs.[45]

Pronounced NIR absorption and high catalytic activity of vdW materials significantly enhance the efficiency of PDT.[111,112] Additionally, vdW nanomaterials with high atomic numbers (e.g., WS_2, Ta_2C) serve as CT contrast agents and RT sensitizers, while those with magnetic properties (e.g., $Cu_{2-x}S$) function as MRI contrast agents.[113,114] The multimodality and synergy with conventional therapies, combined with high biocompatibility and the potential for biodegradation of vdW NPs, appear as a very promising basis for the medicine of the future.[115,116] The ability to engineer their small size and surface chemistry for optimal biodistribution, target specificity, and drug release profiles highlights their potential to revolutionize advanced personalized medicine.

Additive Technologies. Additive manufacturing techniques have revolutionized the production of composite materials, offering a straightforward solution for creating complex, custom-designed shapes. In the biomedical sector, 3D printing has enabled the fabrication of scaffolds tailored to patient-specific needs, allowing for precise control over product architecture and microstructure.[117] Polymers reinforced with graphene or its derivatives have shown significant potential for applications requiring enhanced electrical and mechanical properties and improved cell response, thereby becoming increasingly attractive for biomedical applications.[118] The ability to tailor the properties of vdW NPs through controlled synthesis and functionalization opens avenues for innovation in material design and manufacturing. As research in this field progresses, the integration of vdW NPs into additive technologies is anticipated to drive significant advancements in the fabrication of next-generation devices and systems. Laser-induced forward transfer (LIFT), a technique that involves the use of focused laser pulses to transfer material from a donor to a receiver substrate in a controllable manner, may benefit from using the vdW materials. Recent development in the LIFT technique has led to the controlled fabrication of metallic (Au, Ag, Al, Cu, Fe, etc.) and semiconductor (Si, Ge, etc.) NPs with precisely adjustable radii between 50 nm and 1 μm and their accurate positioning on the desired substrate.[59] The use of vdW films as donor substrates for printing vdW NPs could significantly expand the applications scope of nanophotonic structures produced by LIFT owing to the high refractive index, low ohmic losses, and giant birefringence of many vdW materials.[119] Beyond laser-based techniques, vdW NPs have potential in other additive manufacturing methods. For example, in inkjet printing, the dispersibility and stability of vdW NPs in various solvents can lead to the development of high-performance inks for printing high-refractive index coatings and sensors.

Thermoelectricity. vdW materials are known for their superior thermoelectric (TE) characteristics, attributed to their low dimensionality in electronic and phonon transport. Studies have demonstrated significant enhancements in the TE properties of 2D WSe_2 and WS_2 compared to their bulk counterparts.[120] Other promising materials include $PtSe_2$[121] and $PdSe_2$.[122] It has been suggested that due to a variety of phonon scattering mechanisms and the inherent energy dependency of their electronic density of states, low-dimensional materials may exhibit improved TE performance over bulk materials.[123] The TE efficiency of MoS_2 has also been shown to surpass that of 3D semiconductors.[124] Furthermore, Bi_2S_3 NPs have been explored for their TE properties, showing promise for use in waste heat recovery and cooling applications.[125] The combination of low thermal conductivity and tunable electrical properties positions Bi_2S_3 as a strong candidate for efficient TE materials capable of transforming temperature gradients into electrical energy.[126]

NIR Shielding. The development of efficient NIR shielding materials is crucial for reducing heat absorption and providing protection against NIR radiation, offering substantial benefits in terms of energy conservation and personal safety.[127] The pronounced absorption observed in various vdW materials, such as Bi_2S_3, within the NIR spectrum renders them highly suitable for NIR shielding applications. This characteristic is particularly valuable for the development of protective coatings for buildings or vehicles aimed at diminishing heat intake from sunlight. Such advancements contribute to significant energy savings in air conditioning systems. Integrating an infrared shielding function with photocatalytic materials paves the way for multifunctional materials, envisaged as innovative smart window coatings. Considering the exceptional photocatalytic properties of vdW NPs, their application in NIR shielding coatings emerges as a promising avenue.

Integration of Synthesized Nanoparticles into Target Applications. The successful integration of the synthesized NPs into practical applications relies on their controlled processing and deposition. Since our NPs are dispersed in colloidal solutions, their implementation primarily depends on liquid-phase techniques. Uniform dispersion and maximization of active surface area are crucial for applications requiring high interfacial reactivity, such as catalysis and energy conversion, and can be achieved through techniques like drop-casting, spray coating, or electrophoretic deposition.[128] Precise spatial arrangement and thickness control are essential for functional thin films in electronic and sensing applications, where methods such as inkjet printing, and dip-coating allow for fine-tuned NP placement.[23] Stability in liquid or biological environments is critical for biomedical and colloidal applications, necessitating surface functionalization strategies like PEGylation or lipid coating to ensure biocompatibility and controlled interaction with biological systems.[108] Mechanical reinforcement and tailored optoelectronic properties are key in nanocomposites and printable materials, where NP-polymer integration through solution blending or additive manufacturing enables tunable mechanical strength and functional performance.[118] These processing approaches provide a versatile toolkit for tailoring NP behavior to meet the specific requirements of diverse technological applications.

Beyond Traditional Layered Materials. The pulsed laser ablation in liquids method has demonstrated significant

https://doi.org/10.1021/acsnano.5c00546
ACS Nano 2025, 19, 22820−22836

potential for synthesizing NPs from emerging two-dimensional materials beyond vdW layered crystals. Recent experimental reports have successfully applied this technique to inorganic halide perovskite nanocrystals (e.g., $CsPbBr_3$ via laser ablation in low-boiling-point alcohols under ambient conditions[129]), black phosphorus quantum dots,[130] and antimonene nanosheets.[131] Emerging Xenes, including silicene and germanene, accessible via bottom-up epitaxial growth by molecular beam epitaxy (MBE) or chemical vapor deposition (CVD), or topochemical deintercalation of Zintl phases ($CaSi_2$, $CaGe_2$), provide high-purity layered targets that should be readily convertible into colloidal NPs by laser ablation in liquids.[132,133] Beyond Xenes, other emerging two-dimensional materials such as graphyne and graphdiyne currently lack stable bulk precursors; however, the successful generation of graphene quantum dots by laser ablation suggests that suitably engineered graphyne structures could similarly yield carbon-based nanostructures. Future work will explore optimized ablation parameters and novel precursor designs to further extend this method to these promising material families.

In summary, our approach to producing geometrically precise vdW NPs holds significant promise across a broad range of technological applications due to their unique and tunable properties. Their development and integration into devices and systems have the potential to drive innovations and improve performance in energy, catalysis, medicine, neuromorphic electronics, environmental remediation, and beyond. However, despite the promising prospects, several challenges need to be addressed. These include the scalability of the synthesis process of NPs with controlled size, shape, and composition, as well as ensuring their stability and compatibility in various applications. Another drawback of many powder materials, including NPs, is their challenging recyclability and reusability. This limitation not only contributes to secondary environmental pollution but also incurs significant costs due to the need for complex separation technologies. Continued research and development are crucial to address these challenges and fully exploit the potential of vdW NPs.

CONCLUSIONS

The emergence of advanced technologies for the fabrication of layered vdW materials with diverse compositions and tunable physicochemical properties has broadened their applicability for both scientific research and industrial applications. Due to their synthetic nature, these materials present unprecedented opportunities for developing over 5000 nanostructures that achieve remarkable performance in fields such as energy applications, catalysis, biomedicine, additive manufacturing, nanophotonics, computing, and sensing. Despite these advances, a significant challenge remains in the miniaturization of technologies and functional materials, particularly the lack of a universal method for controllably modifying the dimensional, morphological, and optical properties of vdW nanomaterials while preserving their original composition and stability in dispersed systems.

In this study, we address this challenge by demonstrating the remarkable versatility of the fs laser synthesis method to produce colloidal NPs from vdW materials and perovskites. Our approach allows for precise control over the morphology, size, composition, and optical properties of NPs, achieving high colloidal stability and maintaining the original crystalline structure of over 50 vdW materials. We have shown that laser synthesis can produce a diverse array of nanostructures, including fullerene-like, polygonal, and pyramidal shapes from TMDCs, single-crystalline NPs from M(A)Xenes, and crystalline nanocubes from perovskites. Molecular dynamics simulations further elucidate the crystallization processes involved, revealing that both heterogeneous and homogeneous nucleation mechanisms contribute to the formation of these nanostructures, with the size and core−shell ratio being dependent on the cooling rate.

Thus, this method serves as a tool for fabricating vdW-based NPs and may contribute to future developments in scientific research and technological applications. The ability to create such diverse and well-defined nanostructures paves the way for advancements in numerous fields and offers exciting prospects for future exploration beyond the current applications of layered materials.

METHODS

Laser-Assisted Synthesis of vdW NPs. The colloidal solution of 2D material NPs was prepared using the femtosecond (fs) laser fragmentation and ablation in liquids, similar to our previous studies.[45,64,134,135] A 3 mm beam from Yb:KGW system (1030 nm, 250 fs, up to 400 μJ, 1−200 kHz, TETA-20 model, Avesta, Russia) was used as a laser radiation source. For powdered-type materials, the laser fragmentation technique was used. Here, the reshaping and size reduction processes are based on the interaction of so-called white light supercontinuum irradiation with material (Figure 2a). In case of fragmentation, the initial powder was dispersed in 10−20 mL of acetonitrile (purity ≥ 99.9%, HPLC grade, J.T. Baker, USA) by ultrasonification (5 min) in a glass chamber (BK-7, wall thickness 3 mm). Acetonitrile was used to preserve the original material composition and reduce possible oxidation of the NPs surface, typical for laser synthesis in liquids with a high oxygen content.[42,62] The resulting solution was then irradiated with fs laser pulses, and the focus was adjusted so that the supercontinuum could be generated at 1 cm from the entrance wall of the cuvette. The laser pulses' energy was 50−100 μJ, and the repetition rate was 1−100 kHz. Homogenization of the solution during the fragmentation process was done by magnetic stirrer and manual mixing with a pipet. The concentration of the initial colloidal solution before fragmentation was 0.1 g/L. To increase fragmentation efficiency and utilize most of the volume, we continuously moved the laser beam over the solution using a galvanometric scanner (LScan-10, Ateko TM, Russia) at a speed of 4 m/s. The duration of the laser fragmentation step ranged from 5 to 30 min. The relatively large NPs (>200 nm) were sedimented by a centrifugation step (7500 g, 1 min, liquid height 50 mm, 24 °C) and then fragmented again.

In the case of bulk crystalline materials, the technique of laser ablation in liquids was used. The initial target was fixed vertically in a PTFE stand inside a glass chamber filled with 10−50 mL of acetonitrile. The laser beam was focused on the target surface by the F-Theta lens (63 mm focal distance, Thorlabs, USA). The liquid thickness between the target and chamber wall was minimized to 3 mm to improve the synthesis productivity. The pulse energy was 5−10 μJ, and the repetition rate was 1−200 kHz. To avoid ablation from one spot and increase efficiency, we continuously moved the laser beam over the target surface using the galvanometric scanner at a speed of 5 m/s. The duration of laser ablation was in the range of 5−30 min. The relatively large NPs (>200 nm) were sedimented and removed by a centrifugation step (7500 g, 1 min, liquid height 50 mm, 24 °C).

Characterization of vdW NPs. The size characteristics and atomic composition of the synthesized NPs were studied utilizing a scanning electron microscopy (SEM) system (MAIA 3, Tescan, Czech Republic) operating at 30 kV coupled with an EDX detector (X-act, Oxford Instruments, U.K.). Samples for SEM imaging were prepared by dropping 1−5 μL of the NPs solution onto a cleaned silicon wafer with subsequent drying at ambient conditions.

https://doi.org/10.1021/acsnano.5c00546
ACS Nano 2025, 19, 22820−22836

Morphological and structural properties of synthesized NPs were characterized by the high-resolution TEM system (JEOL JEM 2100, Japan) operating at 200 kV with a GatanMultiscan charge-coupled device in imaging and diffraction modes. Detailed study of the fine structure of the vdW NPs was carried out with the S/TEM (HRTEM, HRSTEM, HAADF) system (Titan Themis Z, Thermo Fisher Scientific, Netherlands) operating at 200 kV, coupled with EDX detector (Super-X, Thermo Fisher Scientific, Netherlands). The Titan Themis Z microscope can correct spherical aberrations, which significantly improves the microscope's resolution. Samples were prepared by dropping 2 μL of NPs solution onto a carbon-coated TEM copper grid and subsequent drying at ambient conditions.

The size distribution of the synthesized NPs was obtained by analysis of the SEM images in the ImageJ software environment with circle fit approximation. The final distribution was based on the measurement of 300−500 NPs diameters.

Hydrodynamic size distribution and Zeta-potential were measured by dynamic light scattering (DLS) and Doppler-anemometry technique, respectively, with Malvern Zetasizer (Nano ZS, Malvern Instruments, U.K.). Mode values ± half-width of the peak of number-weighted size distributions were used as the hydrodynamic diameter. Smoluchowski approximation was used for Zeta-potential calculation.

Molecular Dynamics. MD calculations were performed using the Large-scale Atomic/Molecular Massively Parallel Simulator (LAMMPS) program package[136] with machine-learning interatomic potential MTP.[61] The simulation box with approximate size 203 × 27 × 25 Å^3 contained 6912 atoms (see video of MD simulation in the Supporting Information). Pressure and temperature were controlled via the Nose−Hoover thermostat and barostating.[137] The integration time step was 0.5 fs.

We used an iterative active learning scheme to sample the training data for the interatomic potential MTP. In each iteration, a few atomic configurations of the Mo−S clusters were randomly generated to initialize the parallel sampling from MD trajectories. The sampled configurations were then aggregated into a single list cleaned from duplicates. The energies and interatomic forces were calculated for each configuration using the DFT approach implemented in the VASP package.[138] The training set of the MTP potential was therefore updated, and the potential was retrained on the updated data to start the new sampling iteration. Finally, the sampling was stopped when no new structures were sampled from the MD trajectories for 10 iterations. The resulting training set consisted of 3250 atomic configurations. The error in predicting the energies on the training data was 16 meV/atom.

For the DFT calculations, we used the PBE exchange-correlation functional[139] with PAW pseudopotentials[140] and D3 dispersion corrections.[141] The cutoff energy for plane waves was 600 eV, and a single Γ point was used to sample the first Brillouin zone.

ASSOCIATED CONTENT

Data Availability Statement

The data sets generated and analyzed during the current study are available from the corresponding author upon reasonable request.

Supporting Information

The Supporting Information is available free of charge at https://pubs.acs.org/doi/10.1021/acsnano.5c00546.

Video of the process of core and shell formation in MoS_2 nanoparticle (from MD calculations) (MP4)

Information on synthesized NPs: crystal structure, images of initial crystals/powders/solutions, and TEM images; size, optical, and compositional properties of MoS_2, WS_2, and Ti_3C_2 NPs vs liquid type; zeta potential distribution of laser-synthesized vdW NPs; MD calculation results; and SAED-derived interplanar spacing comparison (PDF)

AUTHOR INFORMATION

Corresponding Author

Valentyn S. Volkov − *Emerging Technologies Research Center, XPANCEO, Dubai, United Arab Emirates;* orcid.org/0000-0001-8994-7812; Email: vsv@xpanceo.com

Authors

Gleb I. Tselikov − *Emerging Technologies Research Center, XPANCEO, Dubai, United Arab Emirates;* orcid.org/0009-0002-0762-015X

Anton A. Minnekhanov − *Emerging Technologies Research Center, XPANCEO, Dubai, United Arab Emirates;* orcid.org/0000-0002-7685-8463

Georgy A. Ermolaev − *Emerging Technologies Research Center, XPANCEO, Dubai, United Arab Emirates;* orcid.org/0000-0002-0895-818X

Gleb V. Tikhonowski − *Emerging Technologies Research Center, XPANCEO, Dubai, United Arab Emirates*

Ivan S. Kazantsev − *Emerging Technologies Research Center, XPANCEO, Dubai, United Arab Emirates*

Dmitry V. Dyubo − *Emerging Technologies Research Center, XPANCEO, Dubai, United Arab Emirates*

Daria A. Panova − *Physics Department, King's College London, London WC2R 2LS, U.K.*

Daniil I. Tselikov − *Emerging Technologies Research Center, XPANCEO, Dubai, United Arab Emirates*

Anton A. Popov − *Emerging Technologies Research Center, XPANCEO, Dubai, United Arab Emirates*

Arslan B. Mazitov − *Emerging Technologies Research Center, XPANCEO, Dubai, United Arab Emirates*

Sergei Smirnov − *Emerging Technologies Research Center, XPANCEO, Dubai, United Arab Emirates*

Fedor Lipilin − *Department of Inorganic Chemistry, University of Chemistry and Technology Prague, 166 28 Prague 6, Czech Republic;* orcid.org/0009-0001-4649-032X

Umer Ahsan − *Department of Inorganic Chemistry, University of Chemistry and Technology Prague, 166 28 Prague 6, Czech Republic*

Nikita D. Orekhov − *Emerging Technologies Research Center, XPANCEO, Dubai, United Arab Emirates*

Ivan Kruglov − *Emerging Technologies Research Center, XPANCEO, Dubai, United Arab Emirates*

Alexander V. Syuy − *Emerging Technologies Research Center, XPANCEO, Dubai, United Arab Emirates*

Andrei V. Kabashin − *Aix-Marseille University, CNRS, LP3, 13288 Marseille, France;* orcid.org/0000-0003-1549-7198

Boris N. Chichkov − *Institute of Quantum Optics, Leibniz Universität Hannover, 30167 Hannover, Germany;* orcid.org/0000-0002-8129-7373

Zdenek Sofer − *Department of Inorganic Chemistry, University of Chemistry and Technology Prague, 166 28 Prague 6, Czech Republic;* orcid.org/0000-0002-1391-4448

Aleksey V. Arsenin − *Emerging Technologies Research Center, XPANCEO, Dubai, United Arab Emirates;* orcid.org/0000-0002-7506-4389

Kostya S. Novoselov − *The University of Manchester, National Graphene Institute, Manchester M13 9PL, U.K.; Department of Materials Science and Engineering, National University of Singapore, Singapore 03-09 EA, Singapore;*

https://doi.org/10.1021/acsnano.5c00546
ACS Nano 2025, 19, 22820−22836

Institute for Functional Intelligent Materials, National University of Singapore, Singapore 117544, Singapore

Complete contact information is available at: https://pubs.acs.org/10.1021/acsnano.5c00546

Author Contributions

G.I.T., A.V.K., B.N.C., A.V.A., K.S.N., and V.S.V. suggested and directed the project. A.A.M., G.A.E., G.V.T., I.S.K., D.V.D., D.A.P., D.I.T., A.A.P., and A.V.S. performed the measurements and analyzed the data. A.B.M., S.S., N.D.O., and I.K., provided theoretical support. Z.S., F.L., and U.A. synthesized part of vdW crystals. G.I.T., A.A.M., G.A.E., G.V.T., I.S.K., and D.A.P. wrote the original manuscript. All authors reviewed and edited the paper. All authors contributed to the discussions and commented on the paper.

Notes

Gleb Tselikov; Anton Minnekhanov; Georgy Ermolaev; Gleb Tikhonowski; Ivan Kazantsev; Dmitry Dyubo; Daria Panova; Daniil Tselikov; Anton Popov; Arslan Mazitov; Sergei Smirnov; Fedor Lipilin; Umer Ahsan; Nikita Orekhov; Ivan Kruglov; Alexander Syuy; Andrei Kabashin; Boris Chichkov; Zdenek Sofer; Aleksey Arsenin; Kostya Novoselov; Valentyn Volkov. Tunable Nanostructuring for van der Waals Materials. 2024, arXiv:2411.14060. arXiv. https://arxiv.org/abs/2411.14060 (accessed May 21, 2025).

The authors declare no competing financial interest.

ACKNOWLEDGMENTS

Z.S. was supported by ERC-CZ program (project LL2101) from Ministry of Education Youth and Sports (MEYS) and by the project Advanced Functional Nanorobots (reg. No. CZ.02.1.01/0.0/0.0/15_003/0000444 financed by the EFRR). A.V.K. acknowledges support from the French government under the France 2030 investment plan, as part of the Initiative d'Excellence d'Aix-Marseille Université—A*MIDEX AMX-22-RE-AB-107 and the French National Research Agency (project ANR-23-CE07-0051). K.S.N. acknowledges support from the Ministry of Education, Singapore (Research Centre of Excellence award to the Institute for Functional Intelligent Materials, I-FIM, project No. EDUNC-33-18-279-V12), the National Research Foundation, Singapore under its AI Singapore Programme (AISG Award No: AISG3-RP-2022-028) and from the Royal Society (U.K., grant number RSRP\R\190000). The authors thank Dr. Valentin Solovey, Elizaveta Gordeeva, and Daria Oliinik for their help in creating the illustrations.

REFERENCES

(1) Wang, Q. H.; Kalantar-Zadeh, K.; Kis, A.; Coleman, J. N.; Strano, M. S. Electronics and Optoelectronics of Two-Dimensional Transition Metal Dichalcogenides. *Nat. Nanotechnol.* **2012**, *7* (11), 699−712.

(2) Mueller, T.; Malic, E. Exciton Physics and Device Application of Two-Dimensional Transition Metal Dichalcogenide Semiconductors. *Npj 2D Mater. Appl.* **2018**, *2* (1), 1−12.

(3) Park, H.; Lee, M.; Wang, X.; Ali, N.; Watanabe, K.; Taniguchi, T.; Hwang, E.; Yoo, W. J. Anisotropic Charge Transport at the Metallic Edge Contact of ReS2 Field Effect Transistors. *Commun. Mater.* **2024**, *5* (1), 1−7.

(4) Liang, S.; Cheng, B.; Cui, X.; Miao, F. Van Der Waals Heterostructures for High-Performance Device Applications: Challenges and Opportunities. *Adv. Mater.* **2020**, *32* (27), No. 1903800.

(5) Burch, K. S.; Mandrus, D.; Park, J.-G. Magnetism in Two-Dimensional van Der Waals Materials. *Nature* **2018**, *563* (7729), 47−52.

(6) Wang, Q. H.; Bedoya-Pinto, A.; Blei, M.; Dismukes, A. H.; Hamo, A.; Jenkins, S.; Koperski, M.; Liu, Y.; Sun, Q.-C.; Telford, E. J.; Kim, H. H.; Augustin, M.; Vool, U.; Yin, J.-X.; Li, L. H.; Falin, A.; Dean, C. R.; Casanova, F.; Evans, R. F. L.; Chshiev, M.; Mishchenko, A.; Petrovic, C.; He, R.; Zhao, L.; Tsen, A. W.; Gerardot, B. D.; Brotons-Gisbert, M.; Guguchia, Z.; Roy, X.; Tongay, S.; Wang, Z.; Hasan, M. Z.; Wrachtrup, J.; Yacoby, A.; Fert, A.; Parkin, S.; Novoselov, K. S.; Dai, P.; Balicas, L.; Santos, E. J. G. The Magnetic Genome of Two-Dimensional van Der Waals Materials. *ACS Nano* **2022**, *16* (5), 6960−7079.

(7) Gish, J. T.; Lebedev, D.; Song, T. W.; Sangwan, V. K.; Hersam, M. C. Van Der Waals Opto-Spintronics. *Nat. Electron.* **2024**, 1−12.

(8) Geim, A. K.; Grigorieva, I. V. Van Der Waals Heterostructures. *Nature* **2013**, *499* (7459), 419−425.

(9) Novoselov, K. S.; Mishchenko, A.; Carvalho, A.; Castro Neto, A. H. 2D Materials and van Der Waals Heterostructures. *Science* **2016**, *353* (6298), aac9439.

(10) Fu, J.-H.; Lu, A.-Y.; Madden, N. J.; Wu, C. C.; Chen, Y.-C.; Chiu, M.-H.; Hattar, K.; Krogstad, J. A.; Chou, S. S.; Li, L.-J.; Kong, J.; Tung, V. Additive Manufacturing Assisted van Der Waals Integration of 3D/3D Hierarchically Functional Nanostructures. *Commun. Mater.* **2020**, *1* (1), 1−10.

(11) Hu, D.; Yang, X.; Li, C.; Liu, R.; Yao, Z.; Hu, H.; Corder, S. N. G.; Chen, J.; Sun, Z.; Liu, M.; Dai, Q. Probing Optical Anisotropy of Nanometer-Thin van Der Waals Microcrystals by near-Field Imaging. *Nat. Commun.* **2017**, *8* (1), 1471.

(12) Ermolaev, G. A.; Grudinin, D. V.; Stebunov, Y. V.; Voronin, K. V.; Kravets, V. G.; Duan, J.; Mazitov, A. B.; Tselikov, G. I.; Bylinkin, A.; Yakubovsky, D. I.; Novikov, S. M.; Baranov, D. G.; Nikitin, A. Y.; Kruglov, I. A.; Shegai, T.; Alonso-González, P.; Grigorenko, A. N.; Arsenin, A. V.; Novoselov, K. S.; Volkov, V. S. Giant Optical Anisotropy in Transition Metal Dichalcogenides for Next-Generation Photonics. *Nat. Commun.* **2021**, *12* (1), 854.

(13) Mooshammer, F.; Chae, S.; Zhang, S.; Shao, Y.; Qiu, S.; Rajendran, A.; Sternbach, A. J.; Rizzo, D. J.; Zhu, X.; Schuck, P. J.; Hone, J. C.; Basov, D. N. In-Plane Anisotropy in Biaxial ReS2 Crystals Probed by Nano-Optical Imaging of Waveguide Modes. *ACS Photonics* **2022**, *9* (2), 443−451.

(14) Vyshnevyy, A. A.; Ermolaev, G. A.; Grudinin, D. V.; Voronin, K. V.; Kharichkin, I.; Mazitov, A.; Kruglov, I. A.; Yakubovsky, D. I.; Mishra, P.; Kirtaev, R. V.; Arsenin, A. V.; Novoselov, K. S.; Martin-Moreno, L.; Volkov, V. S. Van Der Waals Materials for Overcoming Fundamental Limitations in Photonic Integrated Circuitry. *Nano Lett.* **2023**, *23* (17), 8057−8064.

(15) Meng, Y.; Feng, J.; Han, S.; Xu, Z.; Mao, W.; Zhang, T.; Kim, J. S.; Roh, I.; Zhao, Y.; Kim, D.-H.; Yang, Y.; Lee, J.-W.; Yang, L.; Qiu, C.-W.; Bae, S.-H. Photonic van Der Waals Integration from 2D Materials to 3D Nanomembranes. *Nat. Rev. Mater.* **2023**, *8* (8), 498−517.

(16) Verre, R.; Baranov, D. G.; Munkhbat, B.; Cuadra, J.; Käll, M.; Shegai, T. Transition Metal Dichalcogenide Nanodisks as High-Index Dielectric Mie Nanoresonators. *Nat. Nanotechnol.* **2019**, *14* (7), 679−683.

(17) Flöry, N.; Ma, P.; Salamin, Y.; Emboras, A.; Taniguchi, T.; Watanabe, K.; Leuthold, J.; Novotny, L. Waveguide-Integrated van Der Waals Heterostructure Photodetector at Telecom Wavelengths with High Speed and High Responsivity. *Nat. Nanotechnol.* **2020**, *15* (2), 118−124.

(18) Ling, H.; Khurgin, J. B.; Davoyan, A. R. Atomic-Void van Der Waals Channel Waveguides. *Nano Lett.* **2022**, *22* (15), 6254−6261.

(19) Bandurin, D. A.; Mönch, E.; Kapralov, K.; Phinney, I. Y.; Lindner, K.; Liu, S.; Edgar, J. H.; Dmitriev, I. A.; Jarillo-Herrero, P.; Svintsov, D.; Ganichev, S. D. Cyclotron Resonance Overtones and Near-Field Magnetoabsorption via Terahertz Bernstein Modes in Graphene. *Nat. Phys.* **2022**, *18* (4), 462−467.

(20) Anasori, B.; Lukatskaya, M. R.; Gogotsi, Y. 2D Metal Carbides and Nitrides (MXenes) for Energy Storage. *Nat. Rev. Mater.* **2017**, *2* (2), 1−17.
(21) Chaves, A.; Azadani, J. G.; Alsalman, H.; da Costa, D. R.; Frisenda, R.; Chaves, A. J.; Song, S. H.; Kim, Y. D.; He, D.; Zhou, J.; Castellanos-Gomez, A.; Peeters, F. M.; Liu, Z.; Hinkle, C. L.; Oh, S.-H.; Ye, P. D.; Koester, S. J.; Lee, Y. H.; Avouris, P.; Wang, X.; Low, T. Bandgap Engineering of Two-Dimensional Semiconductor Materials. *Npj 2D Mater. Appl.* **2020**, *4* (1), 1−21.
(22) Dean, C. R.; Young, A. F.; Meric, I.; Lee, C.; Wang, L.; Sorgenfrei, S.; Watanabe, K.; Taniguchi, T.; Kim, P.; Shepard, K. L.; Hone, J. Boron Nitride Substrates for High-Quality Graphene Electronics. *Nat. Nanotechnol.* **2010**, *5* (10), 722−726.
(23) Song, O.; Rhee, D.; Kim, J.; Jeon, Y.; Mazánek, V.; Söll, A.; Kwon, Y. A.; Cho, J. H.; Kim, Y.-H.; Sofer, Z.; Kang, J. All Inkjet-Printed Electronics Based on Electrochemically Exfoliated Two-Dimensional Metal, Semiconductor, and Dielectric. *Npj 2D Mater. Appl.* **2022**, *6* (1), 1−12.
(24) Shao, Y.; Wei, L.; Wu, X.; Jiang, C.; Yao, Y.; Peng, B.; Chen, H.; Huangfu, J.; Ying, Y.; Zhang, C. J.; Ping, J. Room-Temperature High-Precision Printing of Flexible Wireless Electronics Based on MXene Inks. *Nat. Commun.* **2022**, *13* (1), 3223.
(25) Sun, L.; Yuan, G.; Gao, L.; Yang, J.; Chhowalla, M.; Gharahcheshmeh, M. H.; Gleason, K. K.; Choi, Y. S.; Hong, B. H.; Liu, Z. Chemical Vapour Deposition. *Nat. Rev. Methods Primer* **2021**, *1* (1), 1−20.
(26) Kabashin, A. V.; Delaporte, Ph.; Pereira, A.; Grojo, D.; Torres, R.; Sarnet, Th.; Sentis, M. Nanofabrication with Pulsed Lasers. *Nanoscale Res. Lett.* **2010**, *5* (3), 454−463.
(27) Castellanos-Gomez, A.; Barkelid, M.; Goossens, A. M.; Calado, V. E.; van der Zant, H. S. J.; Steele, G. A. Laser-Thinning of MoS 2: On Demand Generation of a Single-Layer Semiconductor. *Nano Lett.* **2012**, *12* (6), 3187−3192.
(28) Mupparapu, R.; Steinert, M.; George, A.; Tang, Z.; Turchanin, A.; Pertsch, T.; Staude, I. Facile Resist-Free Nanopatterning of Monolayers of MoS 2 by Focused Ion-Beam Milling. *Adv. Mater. Interfaces* **2020**, *7* (19), No. 2000858.
(29) Munkhbat, B.; Yankovich, A. B.; Baranov, D. G.; Verre, R.; Olsson, E.; Shegai, T. O. Transition Metal Dichalcogenide Metamaterials with Atomic Precision. *Nat. Commun.* **2020**, *11* (1), 4604.
(30) Kabashin, A. V.; Meunier, M. Synthesis of Colloidal Nanoparticles during Femtosecond Laser Ablation of Gold in Water. *J. Appl. Phys.* **2003**, *94* (12), 7941−7943.
(31) Belyaev, I. B.; Zelepukin, I. V.; Kotelnikova, P. A.; Tikhonowski, G. V.; Popov, A. A.; Kapitannikova, A. Yu.; Barman, J.; Kopylov, A. N.; Bratashov, D. N.; Prikhozhdenko, E. S.; Kabashin, A. V.; Deyev, S. M.; Zvyagin, A. V. Laser-Synthesized Germanium Nanoparticles as Biodegradable Material for Near-Infrared Photoacoustic Imaging and Cancer Phototherapy. *Adv. Sci.* **2024**, *11* (20), No. 2307060.
(32) Semaltianos, N. G.; Logothetidis, S.; Perrie, W.; Romani, S.; Potter, R. J.; Sharp, M.; French, P.; Dearden, G.; Watkins, K. G. II−VI Semiconductor Nanoparticles Synthesized by Laser Ablation. *Appl. Phys. A: Mater. Sci. Process.* **2009**, *94* (3), 641−647.
(33) Sajti, C. L.; Sattari, R.; Chichkov, B. N.; Barcikowski, S. Gram Scale Synthesis of Pure Ceramic Nanoparticles by Laser Ablation in Liquid. *J. Phys. Chem. C* **2010**, *114* (6), 2421−2427.
(34) Nolte, S.; Momma, C.; Jacobs, H.; Tünnermann, A.; Chichkov, B. N.; Wellegehausen, B.; Welling, H. Ablation of Metals by Ultrashort Laser Pulses. *J. Opt. Soc. Am. B* **1997**, *14* (10), 2716.
(35) Mafuné, F.; Kohno, J.; Takeda, Y.; Kondow, T.; Sawabe, H. Formation and Size Control of Silver Nanoparticles by Laser Ablation in Aqueous Solution. *J. Phys. Chem. B* **2000**, *104* (39), 9111−9117.
(36) Rehbock, C.; Merk, V.; Gamrad, L.; Streubel, R.; Barcikowski, S. Size Control of Laser-Fabricated Surfactant-Free Gold Nanoparticles with Highly Diluted Electrolytes and Their Subsequent Bioconjugation. *Phys. Chem. Chem. Phys.* **2013**, *15* (9), 3057−3067.
(37) Besner, S.; Kabashin, A. V.; Meunier, M. Two-Step Femtosecond Laser Ablation-Based Method for the Synthesis of Stable and Ultra-Pure Gold Nanoparticles in Water. *Appl. Phys. A: Mater. Sci. Process.* **2007**, *88* (2), 269−272.
(38) Zhang, D.; Gökce, B.; Barcikowski, S. Laser Synthesis and Processing of Colloids: Fundamentals and Applications. *Chem. Rev.* **2017**, *117* (5), 3990−4103.
(39) Sylvestre, J.-P.; Kabashin, A. V.; Sacher, E.; Meunier, M.; Luong, J. H. T. Stabilization and Size Control of Gold Nanoparticles during Laser Ablation in Aqueous Cyclodextrins. *J. Am. Chem. Soc.* **2004**, *126* (23), 7176−7177.
(40) Amendola, V.; Meneghetti, M. Laser Ablation Synthesis in Solution and Size Manipulation of Noble Metal Nanoparticles. *Phys. Chem. Chem. Phys.* **2009**, *11* (20), 3805.
(41) Maximova, K.; Aristov, A.; Sentis, M.; Kabashin, A. V. Size-Controllable Synthesis of Bare Gold Nanoparticles by Femtosecond Laser Fragmentation in Water. *Nanotechnology* **2015**, *26* (6), No. 065601.
(42) Sylvestre, J.-P.; Poulin, S.; Kabashin, A. V.; Sacher, E.; Meunier, M.; Luong, J. H. T. Surface Chemistry of Gold Nanoparticles Produced by Laser Ablation in Aqueous Media. *J. Phys. Chem. B* **2004**, *108*, 16864−16869.
(43) Bärsch, N.; Jakobi, J.; Weiler, S.; Barcikowski, S. Pure Colloidal Metal and Ceramic Nanoparticles from High-Power Picosecond Laser Ablation in Water and Acetone. *Nanotechnology* **2009**, *20* (44), No. 445603.
(44) Streubel, R.; Barcikowski, S.; Gökce, B. Continuous Multigram Nanoparticle Synthesis by High-Power, High-Repetition-Rate Ultrafast Laser Ablation in Liquids. *Opt. Lett.* **2016**, *41* (7), 1486.
(45) Tselikov, G. I.; Ermolaev, G. A.; Popov, A. A.; Tikhonowski, G. V.; Panova, D. A.; Taradin, A. S.; Vyshnevyy, A. A.; Syuy, A. V.; Klimentov, S. M.; Novikov, S. M.; Evlyukhin, A. B.; Kabashin, A. V.; Arsenin, A. V.; Novoselov, K. S.; Volkov, V. S. Transition Metal Dichalcogenide Nanospheres for High-Refractive-Index Nanophotonics and Biomedical Theranostics. *Proc. Natl. Acad. Sci. U. S. A.* **2022**, *119* (39), No. e2208830119.
(46) Kögler, M.; Ryabchikov, Y. V.; Uusitalo, S.; Popov, A.; Popov, A.; Tselikov, G.; Välimaa, A.; Al-Kattan, A.; Hiltunen, J.; Laitinen, R.; Neubauer, P.; Meglinski, I.; Kabashin, A. V. Bare Laser-synthesized Au-based Nanoparticles as Nondisturbing Surface-enhanced Raman Scattering Probes for Bacteria Identification. *J. Biophotonics* **2018**, *11* (7), No. e201700225.
(47) Zelepukin, I. V.; Popov, A. A.; Shipunova, V. O.; Tikhonowski, G. V.; Mirkasymov, A. B.; Popova-Kuznetsova, E. A.; Klimentov, S. M.; Kabashin, A. V.; Deyev, S. M. Laser-Synthesized TiN Nanoparticles for Biomedical Applications: Evaluation of Safety, Biodistribution and Pharmacokinetics. *Mater. Sci. Eng., C* **2021**, *120*, No. 111717.
(48) Zhang, J.; Chaker, M.; Ma, D. Pulsed Laser Ablation Based Synthesis of Colloidal Metal Nanoparticles for Catalytic Applications. *J. Colloid Interface Sci.* **2017**, *489*, 138−149.
(49) Farooq, S.; Vital, C. V. P.; Tikhonowski, G.; Popov, A. A.; Klimentov, S. M.; Malagon, A.G. L.; De Araujo, R. E.; Kabashin, A. V.; Rativa, D. Thermo-Optical Performance of Bare Laser-Synthesized TiN Nanofluids for Direct Absorption Solar Collector Applications. *Sol. Energy Mater. Sol. Cells* **2023**, *252*, No. 112203.
(50) Popov, A. A.; Tselikov, G.; Dumas, N.; Berard, C.; Metwally, K.; Jones, N.; Al-Kattan, A.; Larrat, B.; Braguer, D.; Mensah, S.; Da Silva, A.; Estève, M.-A.; Kabashin, A. V. Laser- Synthesized TiN Nanoparticles as Promising Plasmonic Alternative for Biomedical Applications. *Sci. Rep.* **2019**, *9* (1), 1194.
(51) Kabashin, A. V.; Meunier, M.; Kingston, C.; Luong, J. H. T. Fabrication and Characterization of Gold Nanoparticles by Femtosecond Laser Ablation in an Aqueous Solution of Cyclodextrins. *J. Phys. Chem. B* **2003**, *107* (19), 4527−4531.
(52) Intartaglia, R.; Bagga, K.; Scotto, M.; Diaspro, A.; Brandi, F. Luminescent Silicon Nanoparticles Prepared by Ultra Short Pulsed Laser Ablation in Liquid for Imaging Applications. *Opt. Mater. Express* **2012**, *2* (5), 510.

https://doi.org/10.1021/acsnano.5c00546
ACS Nano 2025, 19, 22820−22836

(53) Ibrahimkutty, S.; Wagener, P.; Menzel, A.; Plech, A.; Barcikowski, S. Nanoparticle Formation in a Cavitation Bubble after Pulsed Laser Ablation in Liquid Studied with High Time Resolution Small Angle X-Ray Scattering. *Appl. Phys. Lett.* **2012**, *101* (10), 103104.
(54) Al-Kattan, A.; Tselikov, G.; Metwally, K.; Popov, A. A.; Mensah, S.; Kabashin, A. V. Laser Ablation-Assisted Synthesis of Plasmonic Si@Au Core-Satellite Nanocomposites for Biomedical Applications. *Nanomaterials* **2021**, *11* (3), 592.
(55) Jung, H. J.; Choi, M. Y. Specific Solvent Produces Specific Phase Ni Nanoparticles: A Pulsed Laser Ablation in Solvents. *J. Phys. Chem. C* **2014**, *118* (26), 14647−14654.
(56) Blandin, P.; Maximova, K. A.; Gongalsky, M. B.; Sanchez-Royo, J. F.; Chirvony, V. S.; Sentis, M.; Timoshenko, V. Yu.; Kabashin, A. V. Femtosecond Laser Fragmentation from Water-Dispersed Microcolloids: Toward Fast Controllable Growth of Ultrapure Si-Based Nanomaterials for Biological Applications. *J. Mater. Chem. B* **2013**, *1* (19), 2489.
(57) Coviello, V.; Forrer, D.; Amendola, V. Recent Developments in Plasmonic Alloy Nanoparticles: Synthesis, Modelling, Properties and Applications. *ChemPhysChem* **2022**, *23* (21), No. e202200136.
(58) Shih, C.-Y.; Streubel, R.; Heberle, J.; Letzel, A.; Shugaev, M. V.; Wu, C.; Schmidt, M.; Gökce, B.; Barcikowski, S.; Zhigilei, L. V. Two Mechanisms of Nanoparticle Generation in Picosecond Laser Ablation in Liquids: The Origin of the Bimodal Size Distribution. *Nanoscale* **2018**, *10* (15), 6900−6910.
(59) Chichkov, B. Laser Printing: Trends and Perspectives. *Appl. Phys. A: Mater. Sci. Process.* **2022**, *128* (11), 1015.
(60) Novikov, I. S.; Gubaev, K.; Podryabinkin, E. V.; Shapeev, A. V. The MLIP Package: Moment Tensor Potentials with MPI and Active Learning. *Mach. Learn. Sci. Technol.* **2021**, *2* (2), No. 025002.
(61) Shapeev, A. V. Moment Tensor Potentials: A Class of Systematically Improvable Interatomic Potentials. *Multiscale Model. Simul.* **2016**, *14* (3), 1153−1173.
(62) Popov, A.; Tikhonowski, G.; Shakhov, P.; Popova-Kuznetsova, E.; Tselikov, G.; Romanov, R.; Markeev, A.; Klimentov, S.; Kabashin, A. Synthesis of Titanium Nitride Nanoparticles by Pulsed Laser Ablation in Different Aqueous and Organic Solutions. *Nanomaterials* **2022**, *12* (10), 1672.
(63) Amendola, V.; Meneghetti, M. What Controls the Composition and the Structure of Nanomaterials Generated by Laser Ablation in Liquid Solution? *Phys. Chem. Chem. Phys.* **2013**, *15* (9), 3027−3046.
(64) Chernikov, A. S.; Tselikov, G. I.; Gubin, M. Yu.; Shesterikov, A. V.; Khorkov, K. S.; Syuy, A. V.; Ermolaev, G. A.; Kazantsev, I. S.; Romanov, R. I.; Markeev, A. M.; Popov, A. A.; Tikhonowski, G. V.; Kapitanova, O. O.; Kochuev, D. A.; Leksin, A. Yu.; Tselikov, D. I.; Arsenin, A. V.; Kabashin, A. V.; Volkov, V. S.; Prokhorov, A. V. Tunable Optical Properties of Transition Metal Dichalcogenide Nanoparticles Synthesized by Femtosecond Laser Ablation and Fragmentation. *J. Mater. Chem. C* **2023**, *11* (10), 3493−3503.
(65) Fromme, T.; Reichenberger, S.; Tibbetts, K. M.; Barcikowski, S. Laser Synthesis of Nanoparticles in Organic Solvents−Products, Reactions, and Perspectives. *Beilstein J. Nanotechnol.* **2024**, *15*, 638−663.
(66) Jendrzej, S.; Gökce, B.; Epple, M.; Barcikowski, S. How Size Determines the Value of Gold: Economic Aspects of Wet Chemical and Laser-Based Metal Colloid Synthesis. *ChemPhysChem* **2017**, *18* (9), 1012−1019.
(67) Monga, D.; Sharma, S.; Shetti, N. P.; Basu, S.; Reddy, K. R.; Aminabhavi, T. M. Advances in Transition Metal Dichalcogenide-Based Two-Dimensional Nanomaterials. *Mater. Today Chem.* **2021**, *19*, No. 100399.
(68) Sharma, S.; Basu, S. Highly Reusable Visible Light Active Hierarchical Porous WO3/SiO2Monolith in Centimeter Length Scale for Enhanced Photocatalytic Degradation of Toxic Pollutants. *Sep. Purif. Technol.* **2020**, *231*, No. 115916.
(69) Fujishima, A.; Honda, K. Electrochemical Photolysis of Water at a Semiconductor Electrode. *Nature* **1972**, *238* (5358), 37−38.
(70) Mehta, A.; Mishra, A.; Basu, S.; Shetti, N. P.; Reddy, K. R.; Saleh, T. A.; Aminabhavi, T. M. Band Gap Tuning and Surface Modification of Carbon Dots for Sustainable Environmental Remediation and Photocatalytic Hydrogen Production−A Review. *J. Environ. Manage.* **2019**, *250*, No. 109486.
(71) Monga, D.; Ilager, D.; Shetti, N. P.; Basu, S.; Aminabhavi, T. M. 2D/2d Heterojunction of MoS2/g-C3N4 Nanoflowers for Enhanced Visible-Light-Driven Photocatalytic and Electrochemical Degradation of Organic Pollutants. *J. Environ. Manage.* **2020**, *274*, No. 111208.
(72) Ermolaev, G. A.; Stebunov, Y. V.; Vyshnevyy, A. A.; Tatarkin, D. E.; Yakubovsky, D. I.; Novikov, S. M.; Baranov, D. G.; Shegai, T.; Nikitin, A. Y.; Arsenin, A. V.; Volkov, V. S. Broadband Optical Properties of Monolayer and Bulk MoS2. *Npj 2D Mater. Appl.* **2020**, *4* (1), 21.
(73) Li, Y.; Wang, H.; Xie, L.; Liang, Y.; Hong, G.; Dai, H. MoS2 Nanoparticles Grown on Graphene: An Advanced Catalyst for the Hydrogen Evolution Reaction. *J. Am. Chem. Soc.* **2011**, *133* (19), 7296−7299.
(74) Ismail, A. F.; Goh, P. S.; Hasbullah, H.; Aziz, F. *Advanced Materials for Wastewater Treatment and Desalination: Fundamentals to Applications*; CRC Press: Boca Raton, 2022. .
(75) Kalantar-Zadeh, K.; Ou, J. Z. Biosensors Based on Two-Dimensional MoS2. *ACS Sens.* **2016**, *1* (1), 5−16.
(76) Kim, H. J.; Lee, J. H. Highly Sensitive and Selective Gas Sensors Using P-Type Oxide Semiconductors: Overview. *Sens. Actuators B Chem.* **2014**, *192*, 607−627.
(77) Joshi, N.; Hayasaka, T.; Liu, Y.; Liu, H.; Oliveira, O. N.; Lin, L. A Review on Chemiresistive Room Temperature Gas Sensors Based on Metal Oxide Nanostructures, Graphene and 2D Transition Metal Dichalcogenides. *Microchim. Acta* **2018**, *185* (4), 213.
(78) Presutti, D.; Agarwal, T.; Zarepour, A.; Celikkin, N.; Hooshmand, S.; Nayak, C.; Ghomi, M.; Zarrabi, A.; Costantini, M.; Behera, B.; Maiti, T. K. Transition Metal Dichalcogenides (TMDC)-Based Nanozymes for Biosensing and Therapeutic Applications. *Materials* **2022**, *15* (1), 337.
(79) Goswami, P.; Gupta, G. Recent Progress of Flexible NO2 and NH3 Gas Sensors Based on Transition Metal Dichalcogenides for Room Temperature Sensing. *Mater. Today Chem.* **2022**, *23*, No. 100726.
(80) Liu, X.; Shuai, H. L.; Liu, Y. J.; Huang, K. J. An Electrochemical Biosensor for DNA Detection Based on Tungsten Disulfide/Multi-Walled Carbon Nanotube Composites and Hybridization Chain Reaction Amplification. *Sens. Actuators B Chem.* **2016**, *235*, 603−613.
(81) Huang, K. J.; Liu, Y. J.; Cao, J. T.; Wang, H. B. An Aptamer Electrochemical Assay for Sensitive Detection of Immunoglobulin e Based on Tungsten Disulfide-Graphene Composites and Gold Nanoparticles. *RSC Adv.* **2014**, *4* (69), 36742−36748.
(82) Huang, K. J.; Shuai, H. L.; Zhang, J. Z. Ultrasensitive Sensing Platform for Platelet-Derived Growth Factor BB Detection Based on Layered Molybdenum Selenide-Graphene Composites and Exonuclease III Assisted Signal Amplification. *Biosens. Bioelectron.* **2016**, *77*, 69−75.
(83) Jariwala, D.; Howell, S. L.; Chen, K. S.; Kang, J.; Sangwan, V. K.; Filippone, S. A.; Turrisi, R.; Marks, T. J.; Lauhon, L. J.; Hersam, M. C. Hybrid, Gate-Tunable, van Der Waals p-n Heterojunctions from Pentacene and MoS2. *Nano Lett.* **2016**, *16* (1), 497−503.
(84) Jiang, H.; Ren, D.; Wang, H.; Hu, Y.; Guo, S.; Yuan, H.; Hu, P.; Zhang, L.; Li, C. 2D Monolayer MoS2-Carbon Interoverlapped Superstructure: Engineering Ideal Atomic Interface for Lithium Ion Storage. *Adv. Mater.* **2015**, *27* (24), 3687−3695.
(85) Zhao, C.; Kong, J.; Yao, X.; Tang, X.; Dong, Y.; Phua, S. L.; Lu, X. Thin MoS2 Nanoflakes Encapsulated in Carbon Nanofibers as High-Performance Anodes for Lithium-Ion Batteries. *ACS Appl. Mater. Interfaces* **2014**, *6* (9), 6392−6398.
(86) Kumar, N.; Mishra, D.; Kumar, A.; Dash, B.; Mishra, R. K.; Song, J.; Jin, S. H. Enhanced Electrochemical Performance of Supercapacitors via Two-Dimensional Indium Sulfide Heterostructure on Carbon Nanotubes. *Appl. Sci. Switz.* **2023**, *13* (6), 3678.

https://doi.org/10.1021/acsnano.5c00546
ACS Nano 2025, 19, 22820−22836

(87) Park, S. K.; Yu, S. H.; Woo, S.; Quan, B.; Lee, D. C.; Kim, M. K.; Sung, Y. E.; Piao, Y. A Simple L-Cysteine-Assisted Method for the Growth of MoS2 Nanosheets on Carbon Nanotubes for High-Performance Lithium Ion Batteries. *J. Chem. Soc., Dalton Trans.* **2013**, *42* (7), 2399−2405.
(88) Wang, Z.; Wu, H.; Burr, G. W.; Hwang, C. S.; Wang, K. L.; Xia, Q.; Yang, J. J. Resistive Switching Materials for Information Processing. *Nat. Rev. Mater.* **2020**, *5* (3), 173−195.
(89) Tang, J.; Yuan, F.; Shen, X.; Wang, Z.; Rao, M.; He, Y.; Sun, Y.; Li, X.; Zhang, W.; Li, Y.; Gao, B.; Qian, H.; Bi, G.; Song, S.; Yang, J. J.; Wu, H. Bridging Biological and Artificial Neural Networks with Emerging Neuromorphic Devices: Fundamentals, Progress, and Challenges. *Adv. Mater.* **2019**, *31* (49), No. 1902761.
(90) Song, M. K.; Kang, J. H.; Zhang, X.; Ji, W.; Ascoli, A.; Messaris, I.; Demirkol, A. S.; Dong, B.; Aggarwal, S.; Wan, W.; Hong, S. M.; Cardwell, S. G.; Boybat, I.; Seo, J. S.; Lee, J. S.; Lanza, M.; Yeon, H.; Onen, M.; Li, J.; Yildiz, B.; del Alamo, J. A.; Kim, S.; Choi, S.; Milano, G.; Ricciardi, C.; Alff, L.; Chai, Y.; Wang, Z.; Bhaskaran, H.; Hersam, M. C.; Strukov, D.; Wong, H. S. P.; Valov, I.; Gao, B.; Wu, H.; Tetzlaff, R.; Sebastian, A.; Lu, W.; Chua, L.; Yang, J. J.; Kim, J. Recent Advances and Future Prospects for Memristive Materials, Devices, and Systems. *ACS Nano* **2023**, *17* (13), 11994−12039.
(91) Liu, P.; Luo, H.; Yin, X.; Wang, X.; He, X.; Zhu, J.; Xue, H.; Mao, W.; Pu, Y. A Memristor Based on Two-Dimensional MoSe2/MoS2 heterojunction for Synaptic Device Application. *Appl. Phys. Lett.* **2022**, *121* (23), 233501.
(92) Zhang, X.; Qiao, H.; Nian, X.; Huang, Y.; Pang, X. Resistive Switching Memory Behaviours of MoSe2 Nano-Islands Array. *J. Mater. Sci. Mater. Electron.* **2016**, *27* (7), 7609−7613.
(93) Yan, Y.; Sun, B.; Ma, D. Resistive Switching Memory Characteristics of Single MoSe2 Nanorods. *Chem. Phys. Lett.* **2015**, *638*, 103−107.
(94) Li, P.; Sun, B.; Zhang, X.; Zhou, G.; Xia, Y.; Gan, L.; Zhang, Y.; Zhao, Y. Effect of Temperature on the Magnetism and Memristive Memory Behavior of MoSe2 Nanosheets. *Mater. Lett.* **2017**, *202*, 13−16.
(95) Jamilpanah, L.; Khademi, I.; Shoa e Gharehbagh, J.; Aziz Mohseni, S.; Mohseni, S. M. Promising Memristive Behavior in MoS2−MoO2−MoO3 Scalable Composite Thin Films. *J. Alloys Compd.* **2020**, *835*, No. 155291.
(96) Kaur, R.; Singh, K. P.; Tripathi, S. K. Electrical, Linear and Non-Linear Optical Properties of MoSe2/PVA Nanocomposites as Charge Trapping Elements for Memory Device Applications. *J. Alloys Compd.* **2022**, *905*, No. 164103.
(97) Kaur, R.; Singh, K. P.; Tripathi, S. K. Study of Linear and Non-Linear Optical Responses of MoSe2−PMMA Nanocomposites. *J. Mater. Sci. Mater. Electron.* **2020**, *31* (22), 19974−19988.
(98) Li, Y.; Cao, J.; Chen, J.; Xu, Q.; Liu, X.; Qiu, J.; Chen, Y.; Wang, H.; Wang, M. Guar Gum-WTe2 Nanohybrid-Based Bio-memristor Synapse With Short- and Long-Term Plasticity. *IEEE Electron Device Lett.* **2023**, *44* (12), 2047−2050.
(99) Pereira, M. E.; Martins, R.; Fortunato, E.; Barquinha, P.; Kiazadeh, A. Recent Progress in Optoelectronic Memristors for Neuromorphic and In-Memory Computation. *Neuromorphic Comput. Eng.* **2023**, *3* (2), No. 022002.
(100) Zhai, Y.; Yang, X.; Wang, F.; Li, Z.; Ding, G.; Qiu, Z.; Wang, Y.; Zhou, Y.; Han, S. T. Infrared-Sensitive Memory Based on Direct-Grown MoS2−Upconversion-Nanoparticle Heterostructure. *Adv. Mater.* **2018**, *30* (49), No. e1803563.
(101) Tian, Y.; Zhang, S.; Tan, W. Improved Optical and Electrical Switching in Bi2S3 Nested Nano-Networks with Broad Trap Distribution. *Appl. Nanosci. Switz.* **2022**, *12* (7), 2023−2030.
(102) Chen, M.; Ki, S. J.; Liang, X. Bi2Se3-Based Memristive Devices for Neuromorphic Processing of Analogue Video Signals. *ACS Appl. Electron. Mater.* **2023**, *5* (7), 3830−3842.
(103) Konstantinova, E. A.; Minnekhanov, A. A.; Trusov, G. V.; Kytin, V. G. Titania-Based Nanoheterostructured Microspheres for Prolonged Visible-Light-Driven Photocatalysis. *Nanotechnology* **2020**, *31* (34), 345207.
(104) Xia, J.; Ge, Y.; Zhao, D.; Di, J.; Ji, M.; Yin, S.; Li, H.; Chen, R. Microwave-Assisted Synthesis of Few-Layered MoS2/BiOBr Hollow Microspheres with Superior Visible-Light-Response Photocatalytic Activity for Ciprofloxacin Removal. *CrystEngComm* **2015**, *17* (19), 3645−3651.
(105) Zou, X.; Zhang, J.; Zhao, X.; Zhang, Z. MoS2/RGO Composites for Photocatalytic Degradation of Ranitidine and Elimination of NDMA Formation Potential under Visible Light. *Chem. Eng. J.* **2020**, *383*, No. 123084.
(106) Li, Q.; Zhang, N.; Yang, Y.; Wang, G.; Ng, D. H. L. High Efficiency Photocatalysis for Pollutant Degradation with MoS 2/C3N4 Heterostructures. *Langmuir* **2014**, *30* (29), 8965−8972.
(107) Chen, H.; Liu, T.; Su, Z.; Shang, L.; Wei, G. 2D Transition Metal Dichalcogenide Nanosheets for Photo/Thermo-Based Tumor Imaging and Therapy. *Nanoscale Horiz.* **2018**, *3* (2), 74−89.
(108) Cheng, L.; Liu, J.; Gu, X.; Gong, H.; Shi, X.; Liu, T.; Wang, C.; Wang, X.; Liu, G.; Xing, H.; Bu, W.; Sun, B.; Liu, Z. PEGylated WS_2 Nanosheets as a Multifunctional Theranostic Agent for in Vivo Dual-Modal CT/Photoacoustic Imaging Guided Photothermal Therapy. *Adv. Mater.* **2014**, *26* (12), 1886−1893.
(109) An, D.; Fu, J.; Zhang, B.; Xie, N.; Nie, G.; Ågren, H.; Qiu, M.; Zhang, H. NIR-II Responsive Inorganic 2D Nanomaterials for Cancer Photothermal Therapy: Recent Advances and Future Challenges. *Adv. Funct. Mater.* **2021**, *31* (32), No. 2101625.
(110) Xu, D.; Li, Z.; Li, L.; Wang, J. Insights into the Photothermal Conversion of 2D MXene Nanomaterials: Synthesis, Mechanism, and Applications. *Adv. Funct. Mater.* **2020**, *30* (47), No. 2000712.
(111) Zhao, Y.; Chen, B.-Q.; Kankala, R. K.; Wang, S.-B.; Chen, A.-Z. Recent Advances in Combination of Copper Chalcogenide-Based Photothermal and Reactive Oxygen Species-Related Therapies. *ACS Biomater. Sci. Eng.* **2020**, *6* (9), 4799−4815.
(112) Liu, G.; Zou, J.; Tang, Q.; Yang, X.; Zhang, Y.; Zhang, Q.; Huang, W.; Chen, P.; Shao, J.; Dong, X. Surface Modified Ti_3C_2 MXene Nanosheets for Tumor Targeting Photothermal/Photodynamic/Chemo Synergistic Therapy. *ACS Appl. Mater. Interfaces* **2017**, *9* (46), 40077−40086.
(113) Zhang, H.; Zeng, X.; Li, Z. Copper-Chalcogenide-Based Multimodal Nanotheranostics. *ACS Appl. Bio Mater.* **2020**, *3* (10), 6529−6537.
(114) Song, X.; Huang, Q.; Yang, Y.; Ma, L.; Liu, W.; Ou, C.; Chen, Q.; Zhao, T.; Xiao, Z.; Wang, M.; Jiang, Y.; Yang, Y.; Zhang, J.; Nan, Y.; Wu, W.; Ai, K. Efficient Therapy of Inflammatory Bowel Disease (IBD) with Highly Specific and Durable Targeted Ta_2C Modified with Chondroitin Sulfate (TACS). *Adv. Mater.* **2023**, *35* (36), No. 2301585.
(115) Shao, J.; Zhang, J.; Jiang, C.; Lin, J.; Huang, P. Biodegradable Titanium Nitride MXene Quantum Dots for Cancer Photo-theranostics in NIR-I/II Biowindows. *Chem. Eng. J.* **2020**, *400*, No. 126009.
(116) Han, X.; Huang, J.; Lin, H.; Wang, Z.; Li, P.; Chen, Y. 2D Ultrathin MXene-Based Drug-Delivery Nanoplatform for Synergistic Photothermal Ablation and Chemotherapy of Cancer. *Adv. Healthc. Mater.* **2018**, *7* (9), 1701394.
(117) Valencia, C.; Valencia, C. H.; Zuluaga, F.; Valencia, M. E.; Mina, J. H.; Grande-Tovar, C. D. Synthesis and Application of Scaffolds of Chitosan-Graphene Oxide by the Freeze-Drying Method for Tissue Regeneration. *Molecules* **2018**, *23* (10), 2651.
(118) Silva, M.; Pinho, I. S.; Covas, J. A.; Alves, N. M.; Paiva, M. C. 3D Printing of Graphene-Based Polymeric Nanocomposites for Biomedical Applications. *Funct. Compos. Mater.* **2021**, *2* (1), 8.
(119) Zotev, P. G.; Wang, Y.; Andres-Penares, D.; Severs-Millard, T.; Randerson, S.; Hu, X.; Sortino, L.; Louca, C.; Brotons-Gisbert, M.; Huq, T.; Vezzoli, S.; Sapienza, R.; Krauss, T. F.; Gerardot, B. D.; Tartakovskii, A. I. Van Der Waals Materials for Applications in Nanophotonics. *Laser Photonics Rev.* **2023**, *17* (8), No. 2200957.
(120) Jobayr, M. R.; Salman, E. M. T. Investigation of the Thermoelectric Properties of One-Layer Transition Metal Dichalcogenides. *Chin. J. Phys.* **2021**, *74*, 270−278.

https://doi.org/10.1021/acsnano.5c00546
ACS Nano 2025, 19, 22820−22836

(121) Lee, W. Y.; Kang, M. S.; Choi, J. W.; Kim, S. H.; Park, N. W.; Kim, G. S.; Kim, Y. H.; Lee, S. K. Alternatingly Stacked Low- and High-Resistance PtSe2/PtSe2 Homostructures Boost Thermoelectric Power Factors. *Adv. Electron. Mater.* **2023**, *9* (8), No. 2300170.
(122) Qin, D.; Yan, P.; Ding, G.; Ge, X.; Song, H.; Gao, G. Monolayer PdSe2: A Promising Two-Dimensional Thermoelectric Material. *Sci. Rep.* **2018**, *8* (1), 2764.
(123) Zhang, J.; Liu, H. J.; Cheng, L.; Wei, J.; Liang, J. H.; Fan, D. D.; Shi, J.; Tang, X. F.; Zhang, Q. J. Phosphorene Nanoribbon as a Promising Candidate for Thermoelectric Applications. *Sci. Rep.* **2014**, *4* (1), 6452.
(124) Ghosh, K.; Singisetti, U. Thermoelectric Transport Coefficients in Mono-Layer MoS2 and WSe2: Role of Substrate, Interface Phonons, Plasmon, and Dynamic Screening. *J. Appl. Phys.* **2015**, *118* (13), 135711.
(125) Tarachand; Okram, G. S.; De, B. K.; Dam, S.; Hussain, S.; Sathe, V.; Deshpande, U.; Lakhani, A.; Kuo, Y. K. Enhanced Thermoelectric Performance of Novel Reaction Condition-Induced Bi2S3-Bi Nanocomposites. *ACS Appl. Mater. Interfaces* **2020**, *12* (33), 37248−37257.
(126) Zhang, Y. X.; Zhu, Y. K.; Song, D. S.; Feng, J.; Ge, Z. H. Excellent Thermoelectric Performance Achieved in Bi2Te3/Bi2S3@Bi Nanocomposites. *Chem. Commun.* **2021**, *57* (20), 2555−2558.
(127) Zhou, Y.; Li, N.; Xin, Y.; Cao, X.; Ji, S.; Jin, P. Cs x WO 3 Nanoparticle-Based Organic Polymer Transparent Foils: Low Haze, High near Infrared-Shielding Ability and Excellent Photochromic Stability. *J. Mater. Chem. C* **2017**, *5* (25), 6251−6258.
(128) Park, Y.; Kang, H.; Jeong, W.; Son, H.; Ha, D.-H. Electrophoretic Deposition of Aged and Charge Controlled Colloidal Copper Sulfide Nanoparticles. *Nanomaterials* **2021**, *11* (1), 133.
(129) Sansoni, S.; Anoè, F. M.; Meneghetti, M. Simple and Sustainable Synthesis of Perovskite-Based Optoelectronic Material: $CsPbBr_3$ Nanocrystals *via* Laser Ablation in Alcohol. *Nanoscale Adv.* **2022**, *4* (23), 5009−5014.
(130) Ren, X.; Zhang, F.; Zhang, X. Synthesis of Black Phosphorus Quantum Dots with High Quantum Yield by Pulsed Laser Ablation for Cell Bioimaging. *Chem.−Asian J.* **2018**, *13* (14), 1842−1846.
(131) Zhao, M.; Wu, J.; Wei, Y.; Chen, J. Preparation of Antimonene by Laser Irradiation in Different Solvents for Optical Limiting. *Opt. Mater.* **2020**, *109*, No. 110132.
(132) Molle, A.; Yuhara, J.; Yamada-Takamura, Y.; Sofer, Z. Synthesis of Xenes: Physical and Chemical Methods. *Chem. Soc. Rev.* **2025**, *54* (4), 1845−1869.
(133) *Xenes: 2D Synthetic Materials beyond Graphene*; Molle, A.; Grazianetti, C., Eds.; Woodhead Publishing series in Electronic and Optical Materials; Woodhead Publishing: Cambridge, MA, 2022.
(134) Bulmahn, J. C.; Tikhonowski, G.; Popov, A. A.; Kuzmin, A.; Klimentov, S. M.; Kabashin, A. V.; Prasad, P. N. Laser-Ablative Synthesis of Stable Aqueous Solutions of Elemental Bismuth Nanoparticles for Multimodal Theranostic Applications. *Nanomaterials* **2020**, *10* (8), 1463.
(135) Hahn, A. Influences on Nanoparticle Production during Pulsed Laser Ablation. *J. Laser MicroNanoengineering* **2008**, *3* (2), 73−77.
(136) Plimpton, S. Fast Parallel Algorithms for Short-Range Molecular Dynamics. *J. Comput. Phys.* **1995**, *117* (1), 1−19.
(137) Evans, D. J.; Holian, B. L. The Nose−Hoover Thermostat. *J. Chem. Phys.* **1985**, *83* (8), 4069−4074.
(138) Kresse, G.; Joubert, D. From Ultrasoft Pseudopotentials to the Projector Augmented-Wave Method. *Phys. Rev. B* **1999**, *59* (3), 1758−1775.
(139) Perdew, J. P.; Burke, K.; Ernzerhof, M. Generalized Gradient Approximation Made Simple. *Phys. Rev. Lett.* **1996**, *77* (18), 3865−3868.
(140) Blöchl, P. E. Projector Augmented-Wave Method. *Phys. Rev. B* **1994**, *50* (24), 17953−17979.
(141) Grimme, S.; Antony, J.; Ehrlich, S.; Krieg, H. A Consistent and Accurate Ab Initio Parametrization of Density Functional Dispersion Correction (DFT-D) for the 94 Elements H-Pu. *J. Chem. Phys.* **2010**, *132* (15), 154104.

https://doi.org/10.1021/acsnano.5c00546
ACS Nano 2025, 19, 22820−22836